CHARACTERISING THE STIFFNESS AND HYSTERESIS OF SINGLE AND DUAL TRUCK TYRES

Thabani Tafadzwa Magweba

A research report submitted to the Faculty of Engineering and the Built Environment, of the University of the Witwatersrand, in partial fulfilment of the requirements for the degree of Master of Science in Engineering.

Johannesburg 2019

DECLARATION

I declare that this research report is my own unaided work, except where otherwise acknowledged. It is being submitted for the Degree of Master of Science in Engineering to the University of the Witwatersrand, Johannesburg. It has not been submitted before for any degree or examination to any other University.

30th day of April 2019

In memory of my brother,

Blessing Mufaro Magweba

ACKNOWLEDGEMENTS

I would like to thank the following people for their assistance during my research:

Prof. Frank Kienhöfer for his immensely valuable supervision, patience and support.

My parents, Mr and Mrs. Magweba for their support, funding and guidance.

Mr. Shaun Riekert, Mr. Andrew Heydenrych and the Wits Mechanical Engineering Laboratory staff for their help in various ways during the laboratory testing.

Mr. Joshua Subel and Mr. Adam Shneier for their guidance and assistance with the test rig.

ABSTRACT

High body accelerations in heavy vehicles can result in discomfort, injury and damage to freight. In combination with the suspension, a tyre absorbs road shocks for the comfort of the driver and passengers and ensures the integrity of freight. Heavy vehicles make use of either single or dual truck tyres. The two configurations possess different stiffness and hysteresis or damping characteristics. These stiffness and hysteresis characteristics influence the body accelerations experienced (i.e. the ride). The purpose of this research project was to characterise and compare the stiffness and hysteresis of single and dual truck tyres. Previous research has modelled tyres as a simple spring and damper and as a rigid or flexible ring connected to the hub with spring and damper elements with no hysteresis in both cases. Models such as the FTire and SWIFT models can model hysteresis but are complicated, have numerous parameters and require the purchase of expensive software. A custom-built rolling road rig was employed to measure the tyre deflections and corresponding loads of a Dunlop 385/65 R22.5 single tyre and Dunlop 315/80 R22.5 dual tyres. A tyre model was developed which included a characteristic deflection term to model hysteresis. The model was verified and its parameters validated using static load-deflection tests, dynamic load-deflection tests and stepped load response tests. The results confirmed that tyres exhibit hysteresis and the proposed model fitted the experimental data well. It was shown that tyres possess a characteristic deflection which is a measure of the spatial rate at which the force versus displacement response transitions into a linear response. The dual configuration has a higher average stiffness (loading – 2.550 kN/mm, unloading – 2.032 kN/mm) than the single configuration (loading – 1.859 kN/mm, unloading – 1.553 kN/mm). When loading, the average characteristic deflection was calculated to be $\beta = 0.02403$ mm (single), $\beta = 0.02901$ mm (dual) and when unloading $\beta = 0.02349$ mm (single), $\beta = 0.02976$ mm (dual).

CONTENTS

ACKNOWLEDGEMENTS ii

ABSTRACT iii

CONTENTS iv

LIST OF FIGURES vi

LIST OF TABLES vii

NOMENCLATURE viii

1. INTRODUCTION 1
   - 1.1. Background 1
   - 1.2. Problem Statement 2
   - 1.3. Research Question 3
   - 1.4. Literature Review 4
   - 1.5. Objectives 13
2. RESEARCH METHOD 14
   - 2.1. Tyre Specifications 14
   - 2.2. Test Rig 14
   - 2.3. Instrumentation 16
   - 2.4. Testing Procedure 18
   - 2.5. Model Development 20
3. DATA PROCESSING 21
4. RESULTS AND DISCUSSION 32
   - 4.1. Model Stiffness (k) Results 32
   - 4.2. Averaged Load - Deflection Tests Results 33
   - 4.3. Model (k) vs Tests (k) Results 34
   - 4.4. Characteristic Deflection (β) Results 35
   - 4.5. Model Fit Results 36
5. CONCLUSIONS 39

6. REFERENCES 40

APPENDICES 42

Appendix A1 – Mounting Part Drawing 42

Appendix A2 – Load Deflection Tests LabView Program 43

Appendix A3 – Step Load Tests LabView Program 44

Appendix B1 – LabView Output Sample 46

Appendix B2 – Axle Load on Tyres Calculations 49

Appendix B3 – Deflection and Slope Calculations 53

Appendix B4 – Rollers to Flat Ground Conversions Derivation 56

Appendix B5 – MATLAB code 59

Appendix B6 – Dial Gauge Measurement 62

Appendix C1 – Averaged Load – Deflection Test Results 64

Appendix C2 – Model Fit Results 68

LIST OF FIGURES

Figure 1: ISO Vertical Comfort Limits (Spivey, 2007)..1
Figure 2: Dual vs Single Wheel Configuration (Malzahn & Kienhöfer, 2014)........................2
Figure 3: AFRC Engineering Dynamic Tyre Test Vehicle (Lines & Young, 1989)................4
Figure 4: Schematic of the Experimental Rig (Taylor *et al.*, 2000) 5
Figure 5: Adapted Rigid Ring Tyre Model (Tounonen *et al.*, 2012).......................................6
Figure 6: Rigid Ring Model (Bin & Xiaobo, 2014)...7
Figure 7: Flexible Ring Tyre Model (Geng *et al.*, 2007)..8
Figure 8: Radial Force Element (Gipser, 2007)...9
Figure 9: FTire Model Belt Elements (Gipser, 2007)..9
Figure 10: SWIFT Model Configuration (Pacejka, 2012)...10
Figure 11: Force-Deflection Behaviour of a Spring (Sayers & Riley, 1996).........................11
Figure 12: Image of the rig (Malzahn & Kienhöfer, 2014) 15
Figure 13: Picture of the rig..15
Figure 14: Axle and Tyre Orientation..16
Figure 15: Laser Displacement Sensor Calibration 16
Figure 16: Accelerometer Voltage vs Time (Single Tyre | 30 kN – 20 kN at 0 km/h)............21
Figure 17: Laser Transducer Voltage vs Time (Single Tyre | 30 kN – 20 kN at 0 km/h) 22
Figure 18: Load Cell Voltage vs Time (Single Tyre | 30 kN – 20 kN at 0 km/h) 22
Figure 19: Single Axle Free Body Diagram 23
Figure 20: Single Axle Schematic 24
Figure 21: Tyre and Rollers Geometry when a Load is Applied...25
Figure 22: Loads vs Time (Single Tyre | 30 kN – 20 kN at 0 km/h) 26
Figure 23: Final Loads vs Time (Single Tyre | 30 kN – 20 kN at 0 km/h)............................27
Figure 24: Acceleration vs Time (Single Tyre | 30 kN – 20 kN at 0 km/h) 28
Figure 25: Displacement vs Time (Single Tyre | 30 kN – 20 kN at 0 km/h).........................29
Figure 26: Load vs Displacement Fit (Single Tyre | 30 kN – 20 kN at 0 km/h)......................30
Figure 27: Acceleration vs Time (Single Tyre | 20 kN – 30 kN at 25 km/h) 30
Figure 28: Load vs Displacement (Single Tyre at 0 km/h)..33
Figure 29: Load vs Displacement Fit (Dual Tyre | 30 kN – 40 kN at 0 km/h) 36
Figure 30: Force Envelop..37

LIST OF TABLES

Table 1: Tyre and Axle Specifications....14
Table 2: Motor Specifications....14
Table 3: Laser Displacement Sensor Specifications....17
Table 4: Accelerometer Specifications....17
Table 5: Load Cell Specifications....18
Table 6: Load-Deflection Test Parameters....19
Table 7: Step Load Test Parameters....19
Table 8: Displacement Results Sample....31
Table 9: Model Stiffness (k) Results....32
Table 10: Model (k) vs Tests (k) Results....34
Table 11: Characteristic Deflection (β) Results....35

NOMENCLATURE

f_s	force value for the current model iteration [N]
d	displacement value for the current model iteration [m]
d_o	deflection value from the previous model time step [m]
f_{so}	force value from the previous model time step [N]
f_{lim}	force corresponding to the upper and lower limit force at d [N]
$f_U(d)$	upper force limit for a deflection (d) [N]
$f_L(d)$	lower force limit for a deflection (d) [N]
β	characteristic deflection parameter (the spatial equivalent of a time constant) [mm]
F_{wc}	force experienced at the wheel centre [kN]
F_{lc}	force applied by the hydraulic cylinder [kN]
δ_{wc}	displacement experienced at the wheel centre [mm]
δ_{mp}	displacement experienced at the measurement point [mm]
I	moment of inertia [m^4]
b_o	length of the outer base [m]
b_i	length of the inner base [m]
h_o	outer height [m]
h_i	inner height [m]
A	cross-sectional area [m^2]
r_o	radius of the outer fillet [m]
r_i	radius of the inner fillet [m]
V	volume of the beam [m^3]
L	length of the beam [m]
W_B	weight of the beam [N]
ρ	density [kg/m^3]
g	acceleration due to gravity [m/s^2]

W_H weight of the wheel hub [N]

m mass of the axle [kg]

W_{BWC} load of the beam on the tyre [N]

δ_f displacement experienced on flat ground [mm]

F_f force experienced on flat ground [N]

F_R load experienced at the roller-tyre contact surface [N]

δ_R displacement experienced at the roller-tyre contact surface [N]

k_{wc} stiffness value determined from the force and displacement values at the wheel centre [N/m]

k_R stiffness determined from the force and displacement values at the roller-tyre contact surface [N/m]

k_f stiffness determined from the force and displacement values on a flat surface [N/m]

R_r radius of the rollers [mm]

R_t unloaded radius of the tyre[mm]

F force values [N]

d displacement values [m]

d_i initial deflection value [m]

F_i force value [N]

k gradient of the envelop (and stiffness) [N/m]

C intercept of the envelop [N]

1. INTRODUCTION

1.1.Background

Driver and passenger comfort are measured using vertical, lateral and longitudinal accelerations as well as pitch, roll and yaw angular accelerations that the bodies within the vehicle experience as the vehicle moves over a rough road. The lower the accelerations, the better the ride comfort (Els *et al.*, 2007). The frequency, direction and duration of exposure to the accelerations are important. The driver and passengers have limits with respect to the magnitude and frequency of the acceleration as well as the exposure duration. Above these limits the ride becomes uncomfortable (Segel *et al.*, 1981).

The total weighted root mean square acceleration is used to evaluate the severity of the magnitude of vehicle vibrations and their resultant effect on humans. A root mean squared (RMS) acceleration value greater than 2 m/s^2 results in an uncomfortable ride and less than 0.315 m/s^2 is comfortable (Wu *et al.*, 2012). Figure 1 illustrates an example of comfort levels with respect to RMS acceleration, frequency and duration levels.

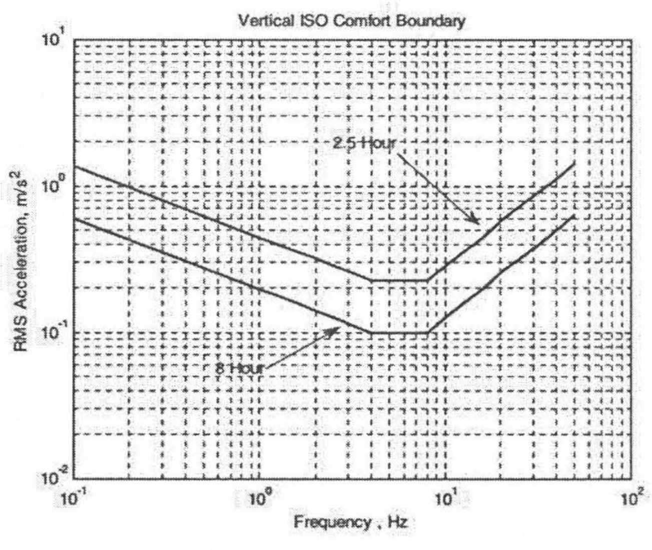

Figure 1: ISO Vertical Comfort Limits (Spivey, 2007)

Driver comfort is influenced by the suspension system and tyres. One of the core functions of the tyre is to absorb road shocks for the comfort of the driver and passengers as well as ensure the integrity of freight (Dugoff *et al.*, 1969) (Lines & Young, 1989). The tyre stiffness and damping influence the vertical acceleration magnitude and frequency (i.e. ride performance) by determining the nature of the transmission of disturbances caused by surface irregularities from the tyre to the passengers. Both the tyre stiffness and damping are influenced by the tyre design characteristics such as tyre material, tread depth and number of plies among others (Wong, 2001).

Commonly used tyre and rim configurations on trucks involve either a single tyre or dual tyres. Figure 2 illustrates the dual and single tyre configurations.

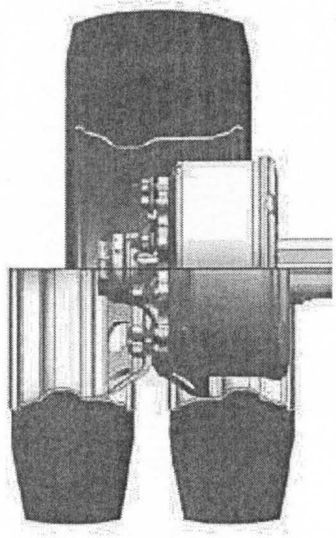

Figure 2: Dual vs Single Wheel Configuration (Malzahn & Kienhöfer, 2014)

The dual configuration is the cheaper and more robust of the two configurations. It eliminates the need for a vehicle to stop in the event of failure of one of the tyres. The single configuration offers weight saving capabilities (Malzahn & Kienhöfer, 2014).

1.2. Problem Statement

Excessive body accelerations as a heavy vehicle traverses over road irregularities can result in discomfort, injury to the driver as well as damage to fragile freight such as glass items. Short exposure usually results in driver fatigue which leads to a decrease in driver performance and prolonged exposure may result in chronic pathological effects such as spinal problems and kidney disease (Segel *et al.*, 1981). It is for this reason that the study of ride, tyre stiffness and tyre hysteresis is important. Dual and single tyres have different stiffness and hysteresis or damping characteristics because of their differences in structural construction, dimensions and configuration during their use. The purpose of this research project was to characterise and compare the stiffness and hysteresis of single and dual truck tyres.

1.3.Research Question

The above problem statement can be formulated into the following research question:

Which tyre configuration possesses higher stiffness and hysteresis values between the single and dual truck tyre configurations? The stiffness is important to understand the ride comfort. The hysteresis is important to understand the rolling resistance and the dissipation of energy. The development of how the stiffness and hysteresis values influence the ride comfort and energy dissipation in the tyres was considered to be beyond the scope of a MSc 50/50 research report.

1.4. Literature Review

Tyres can be modelled as a simple spring and damper or alternatively as a rigid or flexible ring connected to the hub with spring and damper elements. These models do not incorporate hysteresis. Models which include the material properties of the carcass etc (such as the FTire and SWIFT models) can model hysteresis but are complicated and have numerous parameters. As a result, a suspension model called the UMTRI (University of Michigan Transport Research Institute) suspension model which incorporates hysteresis is adapted for modelling tyres.

1.4.1. Characterisation of a Tyre using a Spring and Damper Model

Lines and Young (1989) investigated the tyre stiffness and damping characteristics of a 13.6 x 38 radial tyre using a dynamic test vehicle. Different methods were used to determine the tyre parameters for comparison purposes. These include measuring the load deflection relationship, exciting the system at its natural frequency and measuring the frequencies as well as the rate of decay of the resulting free vibration. Figure 3 shows an image of the machine assembly.

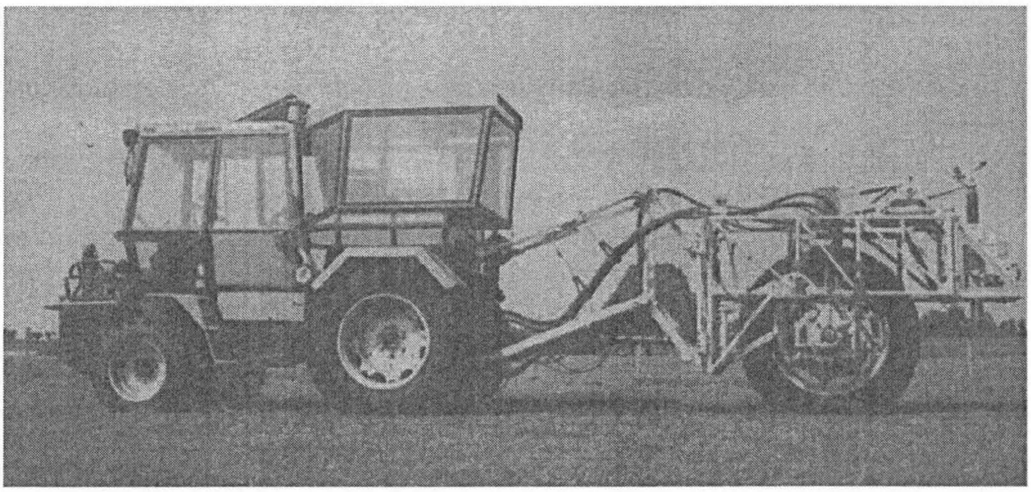

Figure 3: AFRC Engineering Dynamic Tyre Test Vehicle (Lines & Young, 1989)

Hysteresis was observed during the load-deflection testing for which Lines and Young recommended slow load application since the hysteresis was seen to be dependent on the rate of loading and unloading. Lines and Young concluded that tyre parameter values obtained from static tests cannot be used with confidence.

Taylor *et al.* (2000) measured the vertical tyre stiffness of a Goodyear 260/80R20 agricultural tyre using 5 different methods: load-deflection, non-rolling vertical free vibration, non-rolling equilibrium load-deflection, rolling vertical free vibration and rolling equilibrium load-deflection tests. The tests were conducted while the tyre had three different inflation pressures (41, 83 and 124 kPa). The load-deflection method involved measuring the data at the three different pressures by increasing the load exerted, measuring the static load radius and determining the deflection from the difference between the loaded radius and the unloaded radius. The non-rolling and rolling tests involved two methods, the first made use of dropping the tyre from a known elevation and measuring the decay rate of the free vibrations followed by a regression of the vertical position against time data. The second method made use of the equilibrium load-deflection data from the free vibration tests and the deflection was determined from the static load radius after the free vibration had stopped (Taylor *et al.*, 2000). Figure 4 illustrates the experimental rig used.

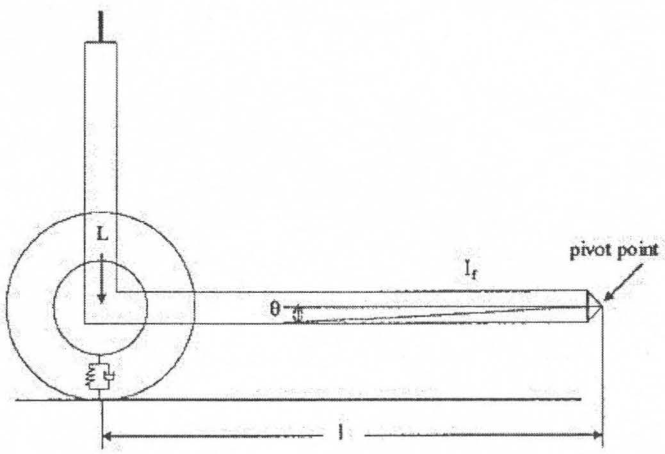

Figure 4: Schematic of the Experimental Rig (Taylor *et al.*, 2000)

Hysteresis was experienced during the experiment. For a tyre modelled as a spring and damper in parallel, Taylor *et al.* (2000) concluded that free vibration should not be used for measurement of the tyre properties and measurements should be made on a rolling wheel at the desired forward velocity.

Lines and Young (1989) and Taylor *et al.* (2000) highlighted the importance of obtaining tyre parameters from a rolling tyre as this produces more accurate results and approximates tyre use better than static tests. Hysteresis was observed and influenced the results in both cases. However, there were no provisions made to model the hysteresis during vibrational tests.

Including hysteresis in the tyre model would allow vibrational tests to characterise the stiffness and damping characteristics (i.e. the ride performance) of a tyre more accurately.

1.4.2. Characterisation of a Tyre using a Rigid Ring Model

Tounonen *et al.* (2012) developed an in-plane rigid ring model and validated its parameters from vehicle measurements based on a 205/55R16 passenger car tyre. The vehicle measurements included cleat testing, coast-down testing and tyre measurements. The effect of the vehicle suspension movement on the observed tyre modes was studied and reproduced in the model. The cleat testing involved driving the vehicle over four 20 mm high and 30 mm wide rectangular cleats and it was performed as a coast-down test while slowing down. The rigid ring model parameters where determined by simulating the rigid ring model rolling over the cleat and the parameters were fit based on the time domain response. Figure 5 illustrates the configuration of the in-plane rigid ring model.

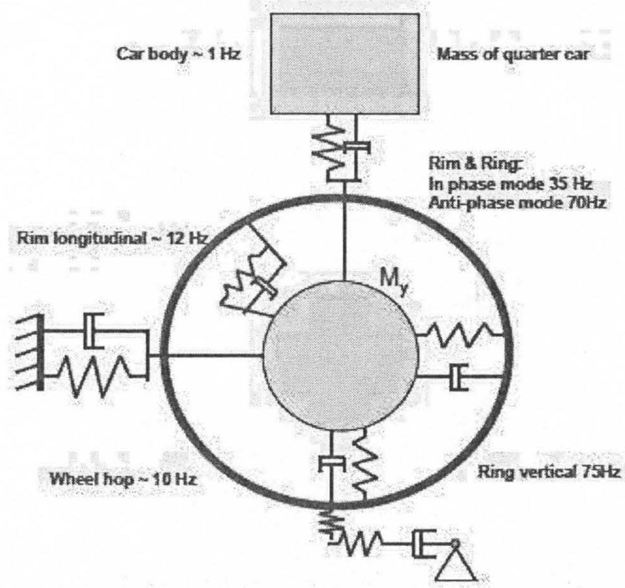

Figure 5: Adapted Rigid Ring Tyre Model (Tounonen *et al.*, 2012)

Tounonen *et al.* concluded that it is possible to characterise the parameters for an in-plane rigid ring model and showed the use of vehicle measurements as a possible method for the characterisation of tyre parameters.

Bin and Xiaobo (2014) developed a simplified rigid ring model as a first step to developing a robust 3-dimensional tyre model. An optimisation technique was used to acquire the necessary tyre parameters of the model by reducing the horizontal and vertical contact forces between the road test data and the model simulation results of the situation of a tyre traversing over a bump. The road test experiment involved the determination of the vertical and longitudinal forces for one tyre as it passes over a round obstacle at a specific velocity. Figure 6 illustrates the developed rigid ring tyre model.

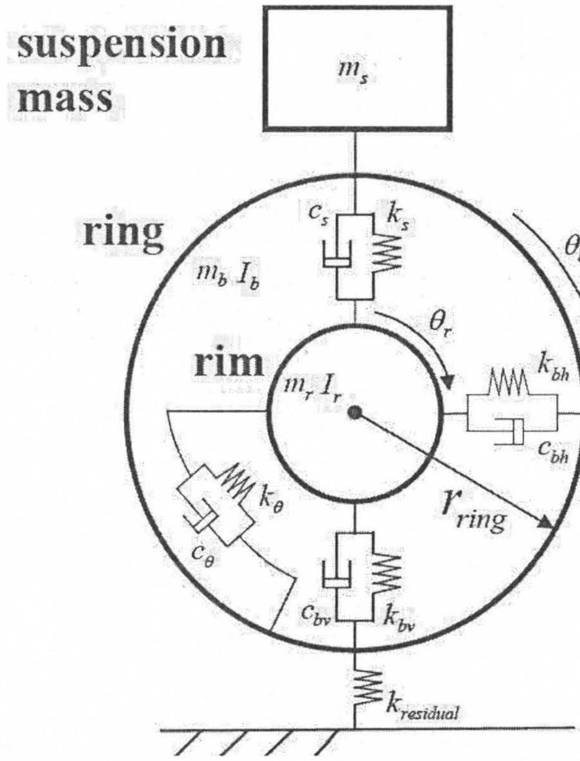

Figure 6: Rigid Ring Model (Bin & Xiaobo, 2014)

Small variations in the velocity during the road test and the round obstacle not being perfectly round were noted as possible sources of inaccuracy. Bin and Xiaobo concluded that the vertical stiffness has the most influence on the forces and since the modelling results depend on the start point as well as the solver, tyre parameter identification needs experimental tests as a guide.

1.4.3. Characterisation of a Tyre using a Flexible Ring Model

Geng *et al.* (2007) investigated the characterisation of tyre properties based on experimental modal analysis. The modal analyses were based on the real and complex modes and the flexible ring model was investigated in conjunction with the real modes to determine its suitability for tyre characterisation. A rig which allows for free vibrations with frequencies that range from 50 Hz to 200 Hz was designed for the tyre testing. The tests were conducted on a Dunlop SP341 295/80R22.5 single truck tyre with inflation pressures from 5.5 bar to 7.5 bar. The experimental technique used involved excitation of the tyre and measurement by an accelerometer. The experimental results were processed based on the real modal analysis and the flexible ring model. Figure 7 illustrates the configuration of the flexible ring model used.

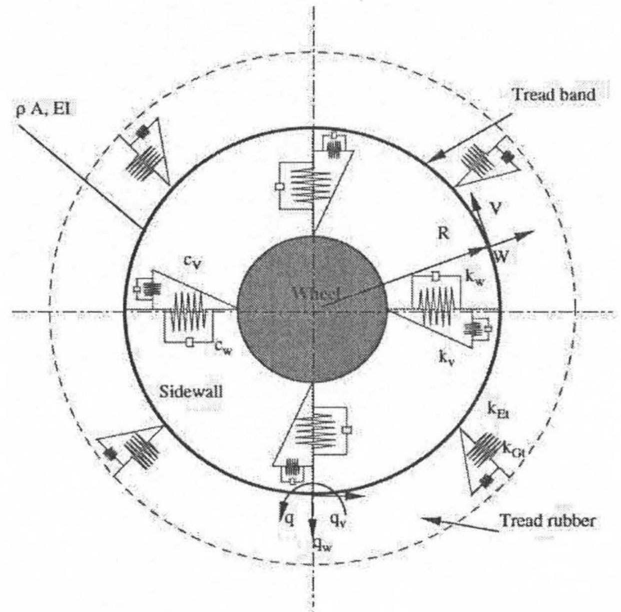

Figure 7: Flexible Ring Tyre Model (Geng *et al.*, 2007)

Geng *et al.* (2007) managed to characterise the tyre parameters using the flexible ring model and its unsuitability between the 150 Hz and 200 Hz frequencies was observed. This was attributed to the failure to describe the physical system of the proportional damping assumption made during the analysis.

1.4.4. The FTire Model

The FTire model is a simulation model designed for use in ride quality simulations and the determination of loads due to road irregularities, with capabilities that extend to handling studies. It is a structural-dynamics-based three-dimensional non-linear tyre model that captures both in and out of plane tyre dynamics during simulation. The tyre belt is modelled as a flexible and extensible ring. Belt elements that are linked by springs and bending stiffnesses approximate the ring and the ring possesses degrees of freedom that allow for in-plane and out-of-plane movements to occur. The bending stiffness values that link the belt elements are a result of partially dynamic lateral, radial and tangential stiffness values. To allow for dynamic stiffening of the overall radial tyre stiffness at high speeds, a parallel connection of a spring and spring-damper series connection refines the radial stiffness between each belt element (Gipser & Hofmann, 2018) (Gisper, 2015) (Gipser, 2007). Figure 8 shows the radial force element of a single belt node.

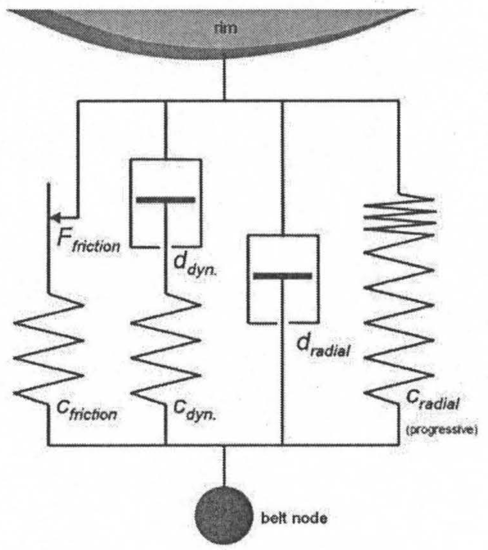

Figure 8: Radial Force Element (Gipser, 2007)

Figure 9 shows the belt elements.

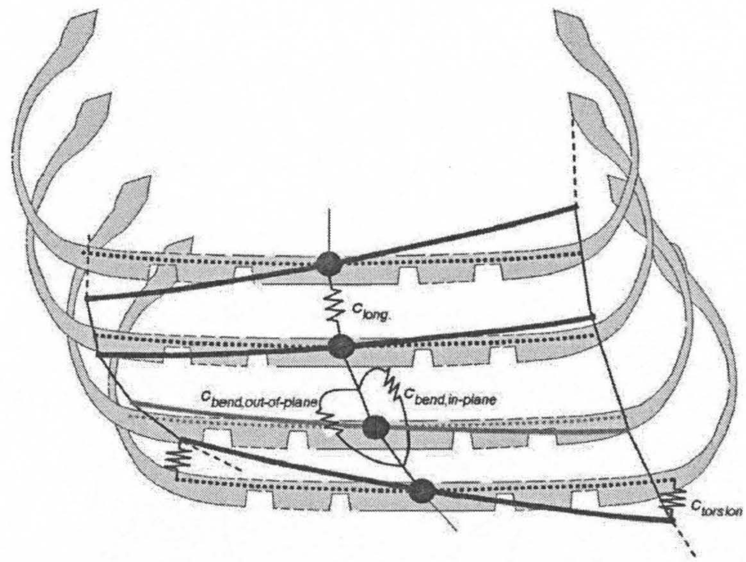

Figure 9: FTire Model Belt Elements (Gipser, 2007)

Five dry friction elements are assembled in parallel to represent the radial hysteresis. A single dry friction element in the tangential direction represents the tangential hysteresis and increase in tyre stiffness at high speeds is described by Maxwell elements. The changes in radial stiffness due to hysteresis as observed during measurements can be seen from FTire based simulations. The model is applicable to vertical, longitudinal and lateral vehicle dynamics situations with very little restriction and it can explain thermodynamic, tribological and mechanical tyre phenomena in line with the results of physical measurements. The FTire model is implemented in software such as FTire (by Cosin software) and ADAMS.

1.4.5. The SWIFT Tyre Model

The SWIFT model (based on the rigid ring type model) is widely regarded as a good model for ride quality assessments. The SWIFT (Short Wavelength Intermediate Frequency Tyre) model can be used in situations where the wavelength is relatively short (>ca. 10 cm), the frequency is relatively high (<ca. 80 Hz) and where the level of slip can be high. The model can describe in-plane and out-of-plane dynamics. The model was originally developed with a restriction to the more important responses to the variations of side slip and longitudinal slip (Pacejka, 2012). The model is based on work supported by TNO Automotive and was conducted at the Delft University of Technology by Maurice and Zegelaar. Components of the model that are unique are: taking into account the inertia of the tyre belt which allows for a proper description of the tyre dynamics, description of moment properties and nonlinear slip force, representation of tyre enveloping behaviour, representation of horizontal thread element compliance and the contact patch and introduction of residual stiffnesses between the ring and the contact patch to make sure that total static tyre stiffnesses in all directions are correct (Pacejka, 2012). A depiction of the configuration of the SWIFT model is shown in Figure 10.

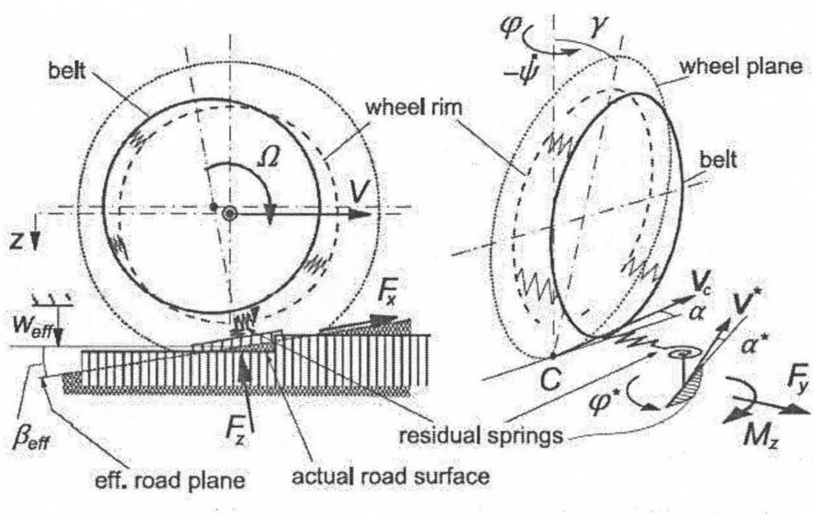

Figure 10: SWIFT Model Configuration (Pacejka, 2012)

The SWIFT model is implemented in computer software such as ADAMS.

1.4.6. Modelling Hysteresis including Characteristic Deflection

The consideration of a tyre as a spring and damper in parallel has been widely used in tyre modelling and the spring element has been proposed to be both non-linear and linear (Taylor *et al.*, 2000). The non-linear portion accounting for the internal damping of the tyre (i.e. hysteresis) which is characteristic of the rubber used to make tyres. Hysteresis causes the tyre to appear stiffer during free vibration since the tyre deflects less for a given load. Lines and Young (1989) and Taylor *et al.* (2000) proposed slower load application to nulify the effects of hysteresis during load-deflecton tests, however this action cannot be implemented during tyre tests that involve vibrational tests with reponse to cleats or impulse loads. The FTire and SWIFT models can model hysteresis but are complicated and have numerous parameters. It is necessary to develop a simple tyre model that accounts for the hysteresis therefore resulting in more accurate tyre parameters when making use of experimental methods or an optimisation technique.

Fancher *et al.* (1980) investigated the force-deflection relationships of several different leaf springs that are used in the suspension systems of commercial vehicles. The work developed a mathematical model to represent the force deflection relationships. Leaf springs dissipate energy during each cycle. Similar behaviour is expected in tyres. The energy dissipation in tyres suggests the presence of hysteresis which the UMTRI model can account for in its representation of the force-deflection relationships. The average damping force is derived from the energy dissipated between loading and unloading. The energy dissipated is equal to the area enclosed within the loading and unloading envelopes which form the hysteresis loop (Fancher *et al.*, 1980). Figure 11 shows an illustration of a hysteresis loop.

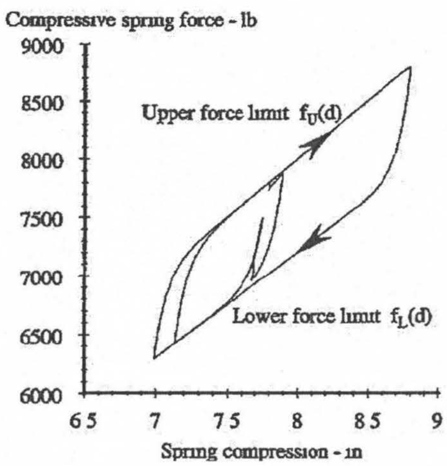

Figure 11: Force-Deflection Behaviour of a Spring (Sayers & Riley, 1996)

The developed model to represent the force-deflection relationship while accounting for hysteresis is denoted by the Equation 1 (Fancher *et al.*, 1980) (Sayers & Riley, 1996).

$$f_s = f_{lim} + (f_{so} - f_{lim})e^{\frac{-|d-d_o|}{\beta}} \quad (1)$$

$$f_{lim} = \begin{cases} f_U(d) & d > d_o \\ f_L(d) & d < d_o \end{cases}$$

Where: f_s and d are the force and displacement values for the current iteration, d_o and f_{so} are the deflection and force values from the previous time step, f_{lim} is the force corresponding to the upper and lower limit force at d , $f_U(d)$ and $f_L(d)$ are the upper and lower force limits for a deflection (d) respectively, in the form of tabular functions and β is the characteristic deflection parameter (the spatial equivalent of a time constant).

1.4.7. The Need for a Simple Tyre Model to Account for Hysteresis

Lines and Young (1989) and Taylor *et al.* (2000) modelled tyres as a spring and damper in parallel and observed hysteresis during load-deflection tests but it was not accounted for during the characterisation of tyres using vibrational tests therefore resulting in discrepancies between the stiffness values obtained from the load-deflection methods and the vibrational analyisis methods. Tounonen *et al.* (2012), Bin and Xiaobo (2014) and Geng *et al.* (2007) showed the use of the rigid ring model and the flexible ring model for the characterisation of tyre parameters as viable methods when coupled together with experimental methods to determine tyre model parameters, however despite the posibility of providing more accurate parameters by the inclusion of more degrees of freedom, the models possess linear spring elements that do not model hysteresis. The FTire model possess elements in its stucture that represent hysteresis in tyres. Hysteresis is modelled using five parameters (radial_hysteresis_force_1-5). However the literature on the FTire model does not have test data illustrating hysteresis in the radial (vertical) or validating the model. Moreover the component or sub-model which captures radial hysteresis has not been clearly published in literature. Futhermore, the implementation of the FTire model requires the purchase of expensive software. The literature on the SWIFT tyre model does not have any details about mechanisms within the model's structure that represent hysteresis and the purchase of expensive software is also required to implement the model.

The spring force-defection model by Fancher *et al.* (1980) is proposed in this research to be applicable to tyre characterisation. The UMTRI model by Fancher can characterise hysteresis without the added complexity of the discretisation of the carcass and it does not require the purchase of expensive and proprietary software.

1.5. Objectives

The objectives are as follows:

- Characterise the stiffness of single truck tyre and dual truck tyre configurations.
- Characterise the hysteresis of single truck tyre and dual truck tyre configurations.

2. RESEARCH METHOD

2.1. Tyre Specifications

The specifications of the tyres on which tests were conducted as well as the details of the axles on which they were mounted are shown in Table 1. The tyres were inflated to a pressure of 7.25 bar.

Table 1: Tyre and Axle Specifications

Component	Manufacturer	Model	Weight
Single tyre	Dunlop	385/65 R22.5 Transteel 883	30 kg
Dual tyre	Dunlop	315/80 R22.5 Transteel 811	50 kg
Single tyre axle	BPW	HSF 9010_15_509	290 kg
Dual tyre axle	BPW	HSF 9010_15_435	305 kg

2.2. Test Rig

A custom-built rig was used, which makes use of linked dual rollers to rotate the single and dual tyres up to a speed of 35 km/h. The rig makes use of a chain drive to transfer power from the motor to the rollers and the overall speed reduction across the chain drive from the motor (see Table 2) to rollers is 1:0.491.

Table 2: Motor Specifications

Power	30 kW
Max Speed	1465 rpm
Rated Torque	196 Nm
Starting Torque	490 Nm

The axle loading frame design allows for free vertical movement while preventing lateral movement to mitigate the risk of failure of the bolts supporting the axle due to the lateral movement. The rig has a safety cage constructed around the tyres, chain drive and rollers to prevent any injury in the case of component failure or tyre blow out. Figure 12 illustrates a schematic of the rig.

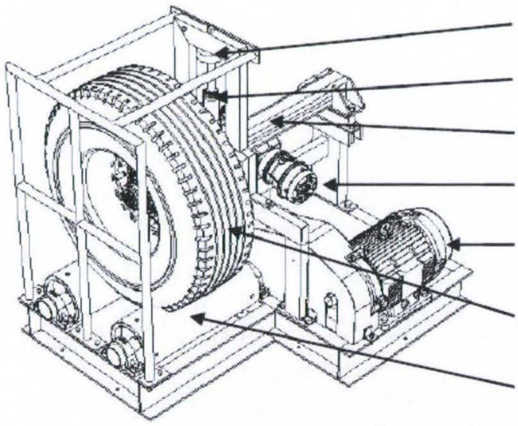

Figure 12: Image of the rig (Malzahn & Kienhöfer, 2014)

Figure 13 shows an image of the rig.

Figure 13: Picture of the rig

The vertical load on the tyre is generated and controlled using a hydraulic piston. The hydraulic piston has a 50 mm bore, a 100 mm stroke and uses a proportional control valve to control the pressure of the fluid moving to the piston. The valve is controlled using a Siemens programmable logic controller that provides the valve with a voltage that corresponds to the required load to be delivered which is measured using the load cell. Siemens Step 7 software is used together with a Siemens 1212C AC/DC relay. A 1.5 kW motor is responsible for driving the system pump that can provide a pressure of 12.83 MPa and a flow rate of 2.9 litres per minute. Figure 14 illustrates the orientation of the axle and tyre combination for the dual tyre case.

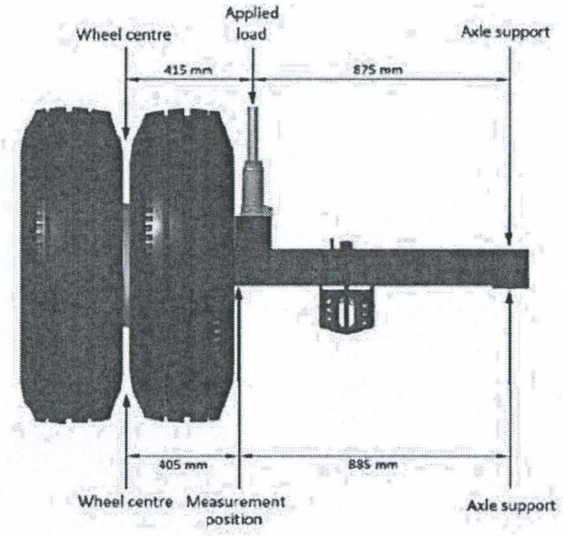

Figure 14: Axle and Tyre Orientation

The single tyre axle is similar but with a total length (wheel centre to axle support) of 1300 mm and an axle support to measurement point distance of 950 mm.

2.3. Instrumentation

Laser Displacement Sensor – A Keyence IL-600 displacement sensor was used for the low bandwidth measurement of the tyre deflection. The sensor was calibrated by creating a table of data consisting of distance against voltage values. The distances within the range of operability of the sensor (200-1000 mm) measured by a tape measure were tabulated against the corresponding sensor voltage values. These data were plotted against each other and the resulting equation was used for the processing of voltages to displacement readings during the testing. The obtained calibration line is shown in Figure 15.

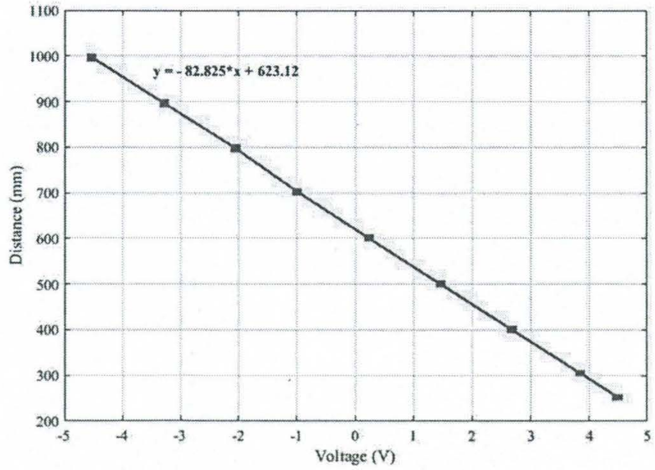

Figure 15: Laser Displacement Sensor Calibration

Table 3 shows the laser displacement sensor specifications (Keyence, 2015).

Table 3: Laser Displacement Sensor Specifications

Make-Model	Keyence IL600
Measurement Range	200 mm - 1000 mm
Sample Rate	0.33/1/2/5 ms
Excitation Voltage	10 – 30 V
Repeatability	50 μm

Accelerometer – A Meggitt 7290E variable capacitance accelerometer was used to obtain measurements of the acceleration experienced by the axles during the tests. The accelerometer was calibrated by collecting the voltage values corresponding to the values of acceleration measured when the accelerometer is in three different positions (i.e. g, 0, -g). These data were plotted against each other and the resulting equation was used for the processing of voltages to acceleration readings during the testing. The primary reason for the acceleration measurements was to determine high bandwidth displacement measurements or tyre deflections using double integration of the accelerations. Table 4 shows the accelerometer specifications (Meggitt, n.d.).

Table 4: Accelerometer Specifications

Make-Model	Meggitt 7290E-2
Measurement Range	+/- 2 g
Sensitivity	1000 (+/- 50) mV/g
Zero Measurand Output	+/- 50 mV
Excitation Voltage	9.5 - 18 V

Load Cell – A separate load cell from the rig load cell used to control the vertical load was used to measure the tyre load. The Zemic (HM2D4-C3-5.0t-5B6-D06) load cell has a full-scale output of 1,9993 mV/V excited at 10 V. A mounting part was designed and added to the actuator piston to ensure it did not slip off. The manufacturing drawing is shown in Appendix A1. Table 5 shows the load cell specifications (Zemic, 2016).

Table 5: Load Cell Specifications

Make-Model	Zemic HM2D4-C3-5.0t-5B6-D06
Capacity	5.0 t
Full Scale Output	1.9993 mV/V
Non-Repeatability	+/- 0.01% of Full Scale
Excitation Voltage	5-12V (nom)

National Instruments Data Acquisition – A National Instruments data acquisition system with a four-slot chassis (NI SCXI-1000) micro controller (NI SCXI-1600) and an eight-channel strain gauge module (NI SCXI-1520) mounted on a terminal block (NI SCXI-1314) was used to acquire the acceleration, load and displacement values measured by the instruments. Programs developed in LabView 2011 were used to facilitate the data acquisition.

2.4. Testing Procedure

2.4.1. Load – Deflection Tests

Axle displacement values were recorded for increasing hydraulic cylinder load values. The load values were varied from 0 kN to a maximum load of 40 kN with load increments of 5 kN. The unloading case was also conducted with axle displacement values being recorded for decreasing hydraulic loads from 40 kN to 0 kN with each decrease being the same magnitude as the increases (i.e. 5 kN). The LabView block diagram for this program is shown in Appendix A2. The axle displacement readings were taken relative to the distance reading from the laser displacement sensor at first contact of the tyre with the rollers when the tyre was being lowered (datum) and the readings with only the axle load acting on the tyre (tyre lowered onto rollers) were included in the data. The load deflection tests were conducted at speeds of 0 km/h, 15 km/h, 25 km/h and 35 km/h. For the dynamic cases, the starting load had to be at least 3 kN as prescribed by the rig operating procedure. Table 6 shows the load deflection test parameters. These tests were conducted for both the single and dual tyre configurations. Each test was conducted three times.

Table 6: Load-Deflection Test Parameters

Test Speeds (km/h)	Test Loads (kN)
0	0 to 40 (+5) and 40 to 0 (-5)
15	5 to 40 (+5) and 40 to 5 (-5)
25	5 to 40 (+5) and 40 to 5 (-5)
35	5 to 40 (+5) and 40 to 5 (-5)

2.4.2. Step Load Response Tests

Step load response load, displacement and acceleration values were collected at various speeds for various initial loads, step load magnitudes and step load directions. The step loads for which responses were collected started from an initial non-zero load. The step loads were applied as an increase in load as well as a decrease in load. The step load was applied by using the manual override function of the rig PLC control program. The manual override percentages entered corresponded to the step load values that were to be tested. The LabView program used to capture the step load response readings from the load cell, laser displacement sensor and the accelerometer is shown in Appendix A3. The readings from the instruments were acquired for 15 seconds at a sample rate of 10 kHz and the collected readings were written to a .lvm file for further processing. The axle displacement readings were taken relative to the distance reading from the laser displacement sensor when the tyre was lowered and stationary (datum). Table 7 shows the test parameters. These tests were conducted for both the single and dual tyre configurations. Each test case was conducted three times. Due to the rig operation procedure, at an initial load of 10 kN, the 10kN decrease was not possible, instead it was a 7 kN decrease.

Table 7: Step Load Test Parameters

Test Speeds (km/h)	Initial Loads (kN)	Step Loads (kN)
0	10, 20, 30	5,10 (Increase and Decrease)
15	10, 20, 30	5,10 (Increase and Decrease)
25	10, 20, 30	5,10 (Increase and Decrease)
35	10, 20, 30	5,10 (Increase and Decrease)

2.5.Model Development

The proposed model that was fitted to the acquired experimental results is based on the model which was developed by Fancher *et al.* (1980) for use in determining the force versus displacement relationship of leaf springs in commercial vehicle suspension systems. The model equation is presented as Equation 2.

$$F = F_i + \left((kd + C) - F_i\right)\left(1 - e^{\frac{-|d-d_i|}{\beta}}\right) \qquad (2)$$

Where: F and d are the force and displacement values, d_i and F_i are the initial deflection and force values (i.e. the start point of the force versus displacement graph), k is the gradient of the envelop (and stiffness), C is the intercept of the envelop and β is the characteristic deflection parameter (the spatial equivalent of a time constant). Equation 2 is in the analytical form of the disrete equation presented by Fancher. Furthermore, the envelop of the force versus displacement graph has been assumed to be linear (i.e $F_{env} = kd + C$).

3. DATA PROCESSING

This section details the steps to process the experimental results. A sample of the raw acceleration, distance and load data collected from LabView during a test is shown in Appendix B1. All the raw data were not presented because the large number of data points (150000) and test cases (288) would result in a large report. Figure 16 shows a plot of the raw accelerometer voltage data obtained during the stationary 30 kN to 20 kN step load test case for the single tyre configuration.

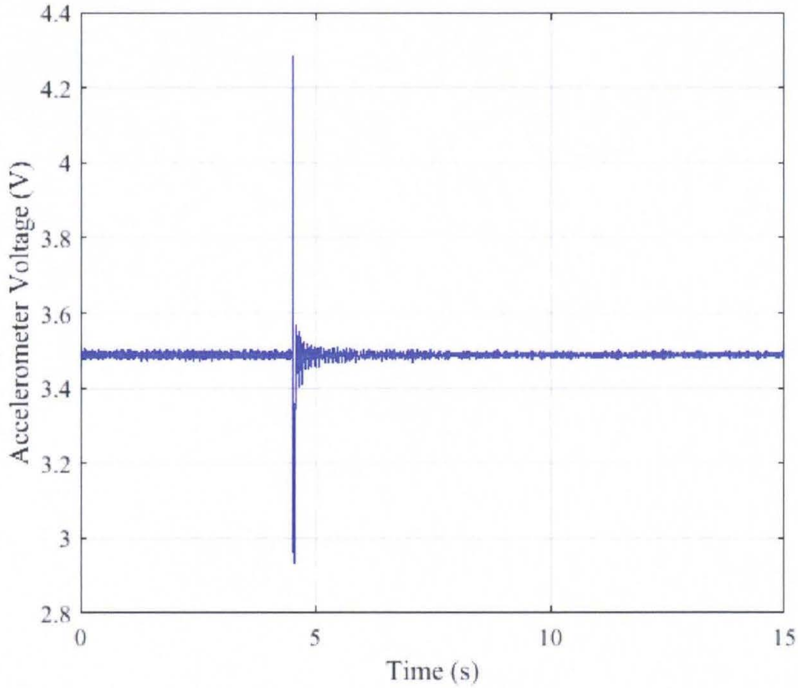

Figure 16: Accelerometer Voltage vs Time (Single Tyre | 30 kN – 20 kN at 0 km/h)

Figure 16 shows a spike in the voltage that corresponds to the load application therefore showing the resulting change in acceleration which can be used to determine the deflection. Figure 17 shows a plot of the raw laser displacement transducer voltage data obtained during the stationary 30 kN to 20 kN step load test case for the single tyre configuration.

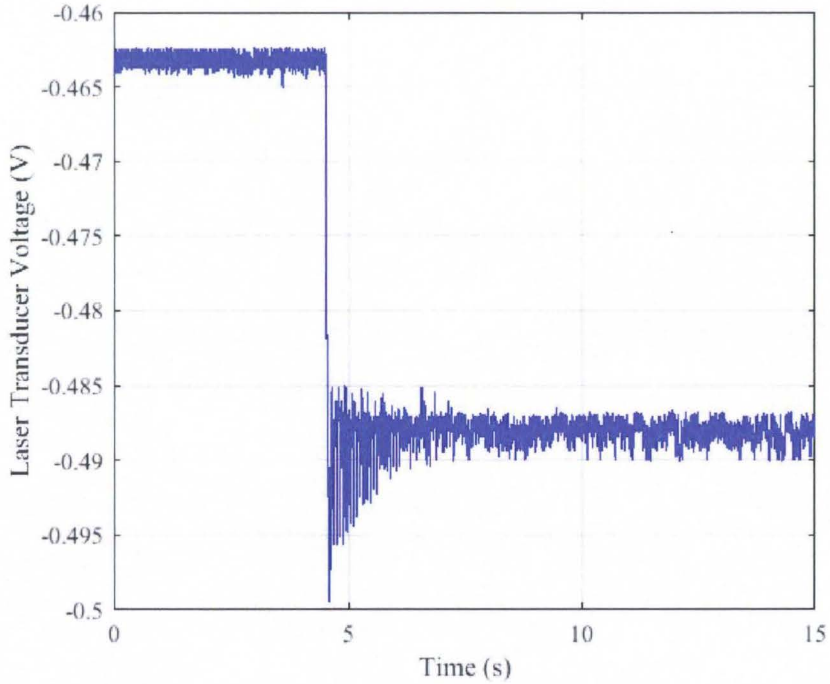

Figure 17: Laser Transducer Voltage vs Time (Single Tyre | 30 kN – 20 kN at 0 km/h)

Figure 17 shows a change in voltage that corresponds to the load application. The change in voltage represents the deflection measured. Figure 18 shows a plot of the load cell voltage data obtained during the stationary 30 kN to 20 kN step load test case for the single tyre configuration.

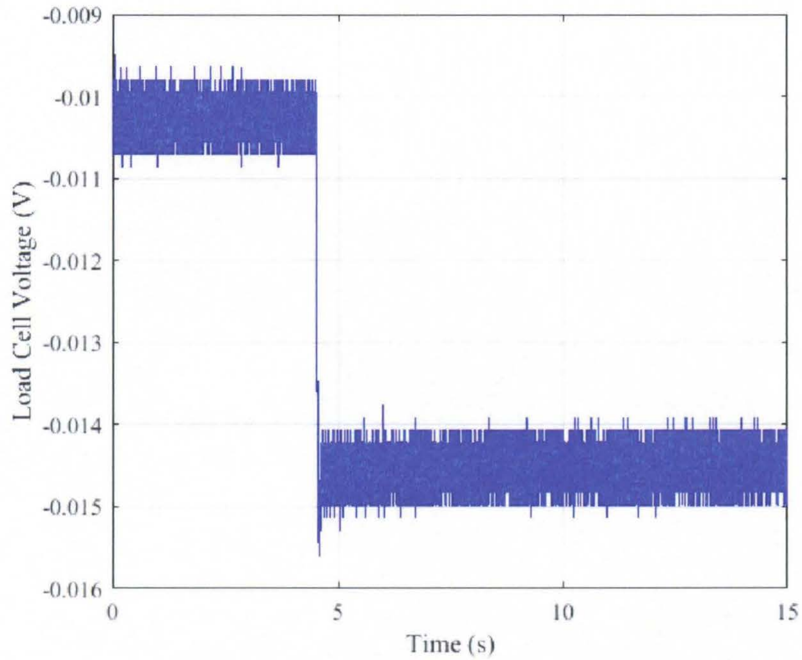

Figure 18: Load Cell Voltage vs Time (Single Tyre | 30 kN – 20 kN at 0 km/h)

Figure 18 shows a change in voltage that corresponds to the load application. The voltage in the plot represents load values. Figures 16 to 18 all show fluctuations in values which are expected to be constant that are attributed to the vibration of the test rig during operation. These voltage values presented in Figures 16 to 18 were converted by the respective calibration equations to give acceleration in m/s^2, displacement in mm and load in kN. It was observed that once the accelerometer and load cell were mounted onto the rig, they produced none zero outputs at rest. Therefore, to shift the LabView calculated acceleration and load values back close to zero, a constant of -9.80725158 was added to the accelerometer calibration equation and a constant of 55.11108 was added to the load cell equation.

The measurement points for the accelerometer and laser displacement transducer as well as the load application point were not at the wheel centre, these data needed to be shifted to the position of the wheel centre. Figure 19 shows a free body diagram of the loading of the single axle with the axle support, wheel centre and load application points shown.

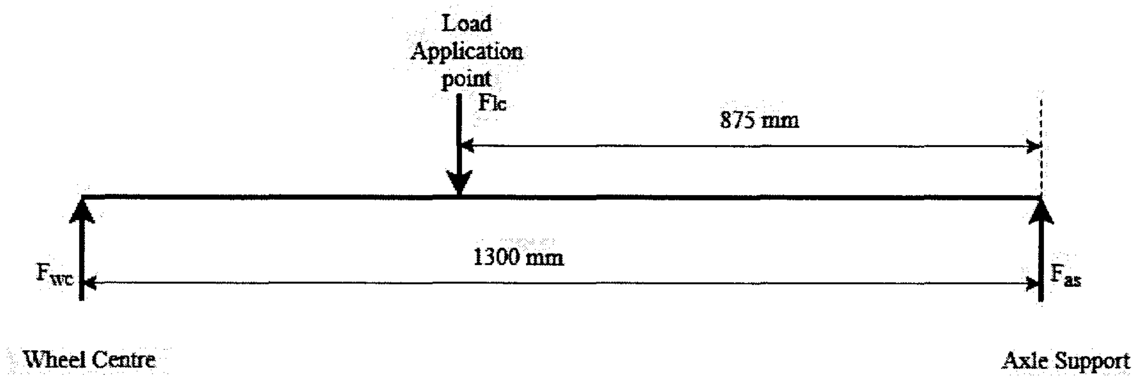

Figure 19: Single Axle Free Body Diagram

The dual axle case possesses a similar free body diagram with the only difference being the length of the axle (1290 mm). Therefore, Equations 3 and 4 were used to calculate the loads experienced at the wheel centre for the single and dual tyre cases respectively.

$$F_{wc} = \frac{875}{1300} F_{lc} \qquad (3)$$

$$F_{wc} = \frac{875}{1290} F_{lc} \qquad (4)$$

Where: F_{wc} is the force experienced at the wheel centre and F_{lc} is the force applied by the hydraulic cylinder. The load experienced by the tyres was a combination of the load applied by the hydraulic cylinder as well as the weight of the wheel and the correct proportion of the axle. Consequently, this weight needs to be added to the force at the wheel centre. The calculations to determine the axle weight acting at the wheel centre are presented in Appendix B2.

Figure 20 shows a schematic of the single axle with regard to the measurement location.

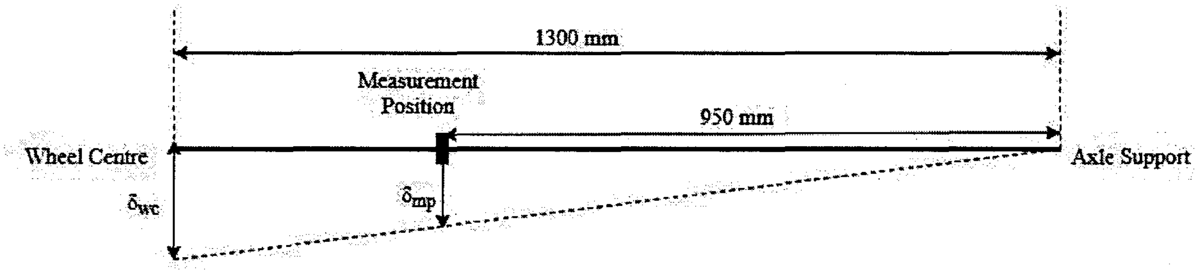

Figure 20: Single Axle Schematic

The dual tyre case possesses a similar schematic with differences in the length of the axle (1290 mm) and the distance between the measurement position and the axle support (885 mm). Therefore, based on similar triangles, Equations 5 and 6 were used to calculate the displacement experienced at the wheel centre for the single and dual tyre cases respectively.

$$\delta_{wc} = \frac{1300}{950}\delta_{mp} \qquad (5)$$

$$\delta_{wc} = \frac{1290}{885}\delta_{mp} \qquad (6)$$

Where: δ_{wc} is the displacement experienced at the wheel centre and δ_{mp} is the displacement experienced at the measurement point. Beam deflection calculations were done to validate the use of similar triangles which assume the axle remains a straight line and to check that the laser displacement sensor values were not affected by axle deflection during loading. The axle deflections and slopes were negligible. These calculations are shown in Appendix B3.

The experiment was conducted while the tyres were on rollers and this does not represent a real-world scenario of a truck moving on a flat road. The relationships between force and deflection on a flat ground are required, therefore the displacement and forces at the wheel centre calculated using equations 3 to 6 were converted to values as if the testing was conducted on flat ground. Figure 21 shows a schematic of the rig geometry when a load is applied.

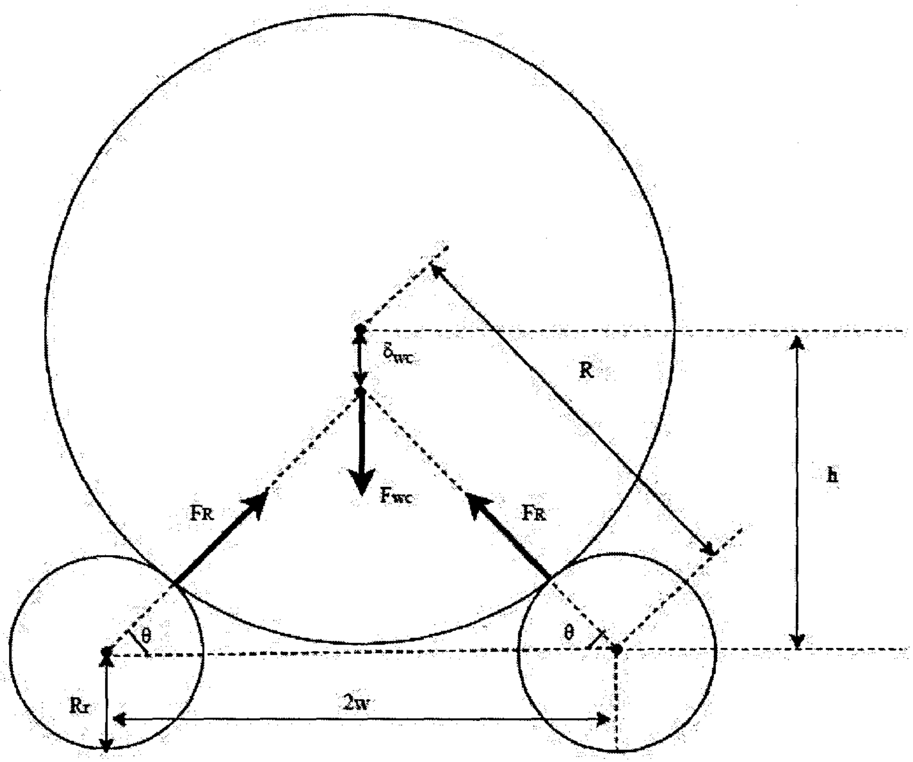

Figure 21: Tyre and Rollers Geometry when a Load is Applied

Equations 7 to 9 where derived for the conversion of the displacement and force from rollers to flat ground. The displacement conversion equation is the same for the single and dual tyre cases, but the force conversion equations for the single and dual tyre cases are slightly different because of the slightly different radii.

$$\delta_f = \delta_{wc} \sin\theta \tag{7}$$

Single:

$$F_f = \frac{F_{wc}}{1.168 \sin\theta} \tag{8}$$

Dual:

$$F_f = \frac{F_{wc}}{1.167 \sin\theta} \tag{9}$$

Sin θ is calculated using Equation 10.

$$\sin\theta = \frac{h - \delta_{wc}}{\sqrt{(h - \delta_{wc})^2 + w^2}} \qquad (10)$$

Where: δ_f is the displacement experienced on flat ground and F_f is the force experienced on flat ground. The derivation of the conversion equations is shown in Appendix B4. Further processing was done using MATLAB.

After the conversions of the measured loads and displacements to those that would be experienced if the tyres were on a flat surface, the values from the three tests conducted for each case were averaged and force versus displacement graphs were plotted using MATLAB from the averaged data obtained during the load-deflection tests. The equations for the lines of best fit for the loading and the unloading data were determined.

For the step response data files, after the conversion, a MATLAB code was written and the files were processed further using MATLAB. The illustration of the processing steps taken in the rest of this section is based on the stationary 30 kN to 20 kN step load test case for the single tyre configuration.

The first step was to ensure that the parts of the code relevant to the first processing step were active and the rest were commented out as well as entering the correct name for the data file to be processed. The load data for the test case were plotted. Figure 22 shows the resulting plot.

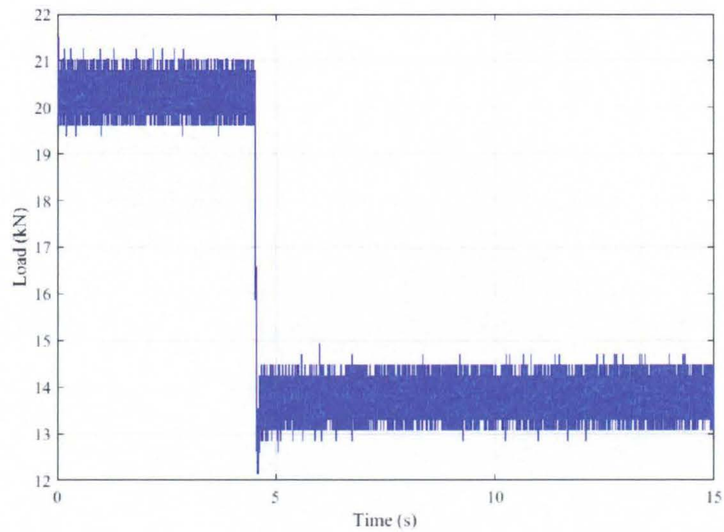

Figure 22: Loads vs Time (Single Tyre | 30 kN – 20 kN at 0 km/h)

Figure 22 shows the plot obtained from applying the load cell calibration equation and the derived conversion equations to the raw load cell voltage plot presented in Figure 18. Averages before and after the step change in load were taken and based on these averages, start and end times of the response where read off the graph with the aid of zooming in. For the start point, the time at which the last spike occurred before the average of the oscillations became greater than the calculated average was taken as the start point. And for the end point, the time at which the first spike occurred after crossing the average was taken as the end point. This eliminated the overshoot observed in the negative step load test cases. The noisy regions before and after the start and end points respectively were all replaced by the calculated average and the noise within the response region was smoothed out by means of a moving average function. Figure 23 shows the resulting load vs time graph.

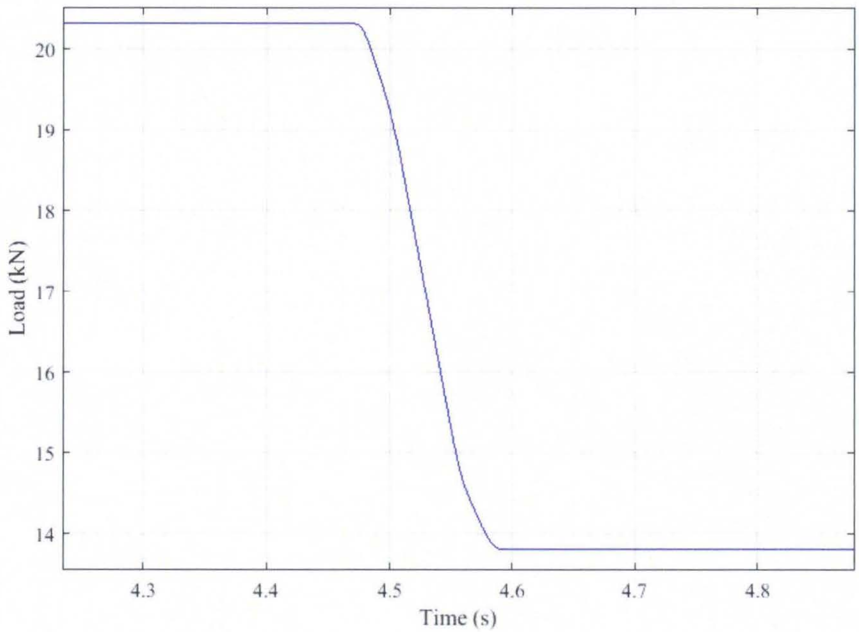

Figure 23: Final Loads vs Time (Single Tyre | 30 kN – 20 kN at 0 km/h)

The average acceleration was subtracted from the acceleration values to zero the acceleration distribution. The acceleration data were plotted and Figure 24 shows the resulting plot.

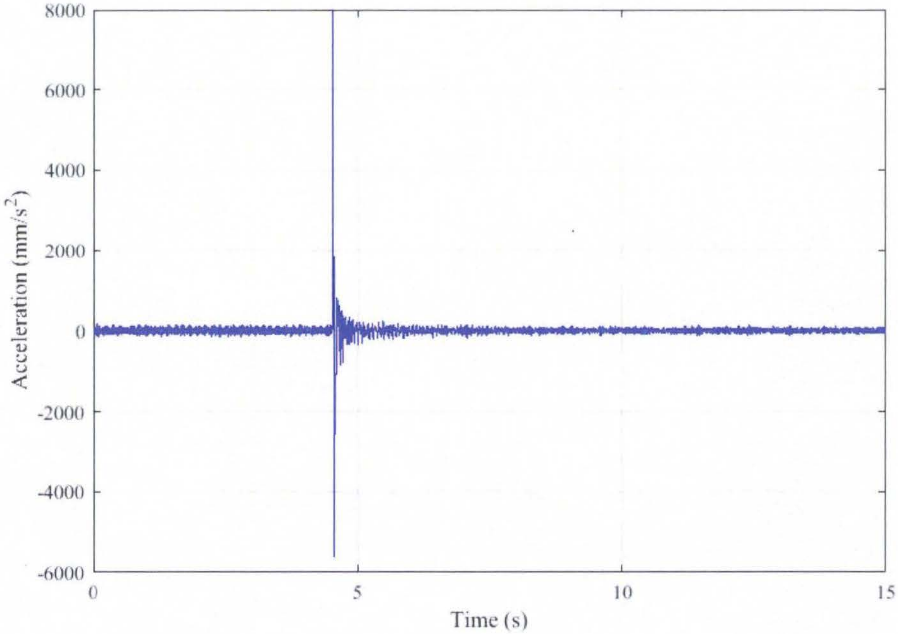

Figure 24: Acceleration vs Time (Single Tyre | 30 kN – 20 kN at 0 km/h)

Figure 24 shows the plot obtained from applying the accelerometer calibration equation and the derived conversion equations to the raw accelerometer voltage plot presented in Figure 16 after zeroing. The start point of the response was taken as the point when the last sign change occurs before the acceleration spike and every value before the start point was replaced by 0. The acceleration was then integrated twice to get displacement. The displacement vs time data were plotted and the displacement value of the first minimum after the overshoot was noted. The time point before the overshoot that corresponds to this displacement value was taken as the end point of the distribution and every value after this point was replaced with the value obtained from the first minimum. This eliminated the overshoot. For the positive step load cases this was not necessary and the first maximum was taken as the end point of the response. After the replacement, the displacement response was smoothed over by means of the same moving average function as the load response and the displacement conversions (Equations 5 and 7) were applied to the data. Figure 25 shows the resulting displacement response.

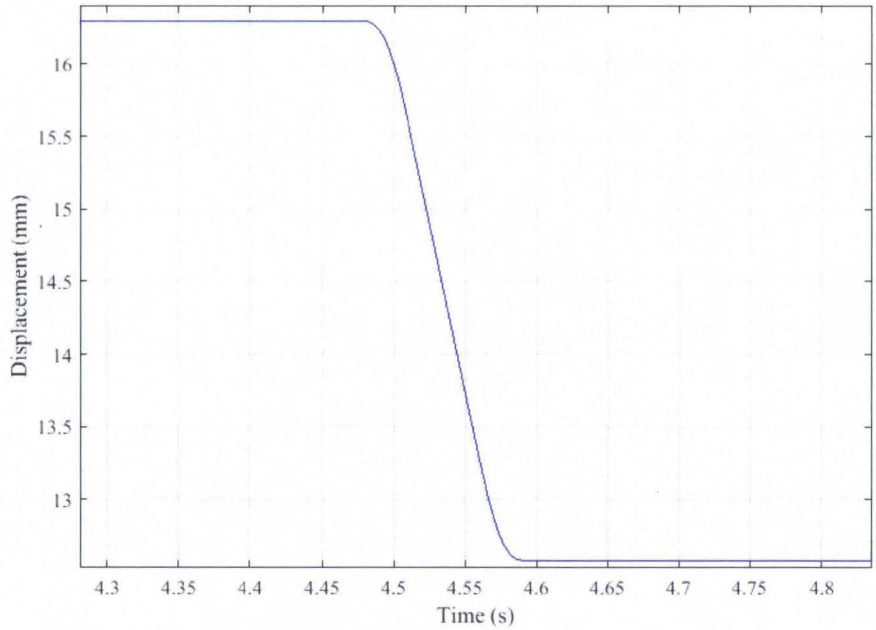

Figure 25: Displacement vs Time (Single Tyre | 30 kN – 20 kN at 0 km/h)

The response regions for the load and displacement data were then isolated by only taking the data within the region denoted by the start time for the load (since the load cell is expected to respond to the step load first) and the end time of the displacement (since the accelerometer was expected to lag). These start and end times where shifted back and forward respectively by half the moving average function value which was 801 (i.e. the actual start time was the original start time minus 400 times the timestep and vice versa for the end time). This is because after applying a moving average that takes the average of 400 points on both sides of a data point (i.e. 801), the 400th point before the original start point includes the value of the start point in its average therefore becoming the new start point. For this reason, the smoothing of the load response and displacement response were done using the same value to maintain consistency.

The loads vs displacement data were then plotted and the developed model was optimised against these data. A portion of the response region was isolated further until a good fit was achieved. All the processed data and results were written to an excel file. Figure 26 shows the fit achieved in this case.

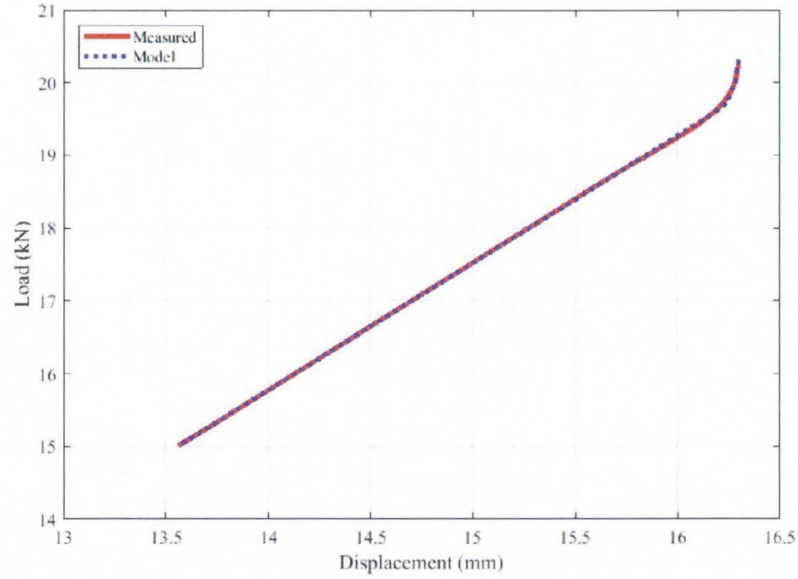

Figure 26: Load vs Displacement Fit (Single Tyre | 30 kN – 20 kN at 0 km/h)

The code used for the MATLAB processing is shown in Appendix B5. The code was used with part of it commented out according to the steps as indicated in the code comments.

The MATLAB processing was applied to all cases except those with excessive amounts of noise and load variations due to the tests being conducted while the tyres were rotating. Because of the noise, the acceleration spike could not be located therefore the processing could not be done. Figure 27 below shows the acceleration plot for such a case.

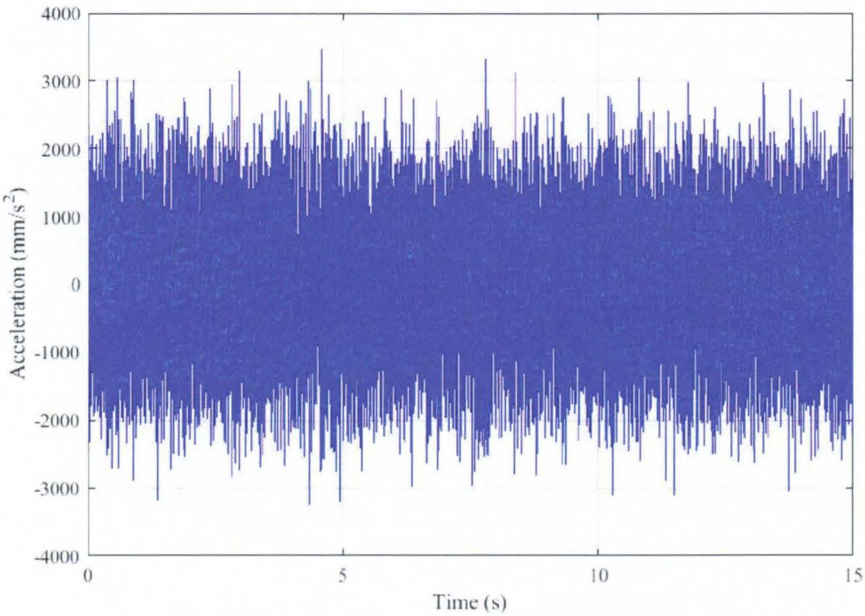

Figure 27: Acceleration vs Time (Single Tyre | 20 kN – 30 kN at 25 km/h)

Attempts to filter the acceleration data were made by making use of the moving mean and a Butterworth filter but since the noise and spike frequencies were so close, the filtering distorted the acceleration peak values therefore rendering the processing procedure invalid. As a result, the processing and results were only produced for cases where the acceleration spike was clearly distinguishable from the noise. These included the positive step load cases at 0 km/h, the negative step load cases at 0km/h and the -5 kN and -10 kN step loads for the 20 kN and 30 kN initial loads at 15 km/h, 25 km/h and 35 km/h.

Every test case was conducted thrice and averages were calculated from the results obtained (i.e. β and k). If one value was significantly different from the other two values, it was not included in the average.

Reliability

A sample test was conducted which involved the application of a 10kN step load. The deflection during the sample test was determined from the integration of the acceleration versus time graph obtained when the step load was applied and a dial gauge positioned against the rig axle. An average value of 3.28 mm was obtained from the dial gauge and a value of 3.05 mm was obtained from the acceleration integration. The percentage difference between the values was judged to be within acceptable limits. Images showing the dial gauge measurement are shown in Appendix B6.

Each of the test cases detailed in Table 7 was conducted three times during the laboratory tests and the repeatability of the experimental testing and data processing methods was satisfactory. Table 8 shows that acceptable repeatability was obtained for the displacement readings.

Table 8: Displacement Results Sample

Configuration	**Test Speed (km/h)**	**Step Load (kN)**	**Displacement (mm)**		
			Test 1	**Test 2**	**Test 3**
Single Tyre	0	10-20	3.418	3.318	3.608
	25	30-25	1.863	1.942	1.604
Dual Tyre	0	10-15	1.366	1.441	1.474
	25	30-20	3.158	2.742	2.607

4. RESULTS AND DISCUSSION

4.1.Model Stiffness (k) Results

Table 9 shows the model stiffness (k) values obtained for each of the processed cases.

Table 9: Model Stiffness (k) Results

Up			Down		
	Singles	**Duals**		**Singles**	**Duals**
(km/h) kN	**k (kN/mm)**	**k (kN/mm)**	**k (kN/mm)**	**k (kN/mm)**	**k (kN/mm)**
(0)10-15	1.703	2.379	**(0)10-3**	1.710	1.945
(0)10-20	1.703	2.283	**(0)10-5**	1.622	2.074
(0)20-25	1.877	2.497	**(0)20-10**	1.698	2.143
(0)20-30	1.938	2.485	**(0)20-15**	1.647	2.346
(0)30-35	1.962	2.843	**(0)30-20**	1.725	2.265
(0)30-40	1.969	2.815	**(0)30-25**	1.746	2.554
			(15)20-10	1.494	1.834
			(15)20-15	1.479	1.639
			(15)30-20	1.481	1.859
			(15)30-25	1.527	1.934
			(25)20-10	1.575	2.096
			(25)20-15	1.592	1.710
			(25)30-20	1.486	1.940
			(25)30-25	1.521	2.706
			(35)20-10	1.475	1.497
			(35)20-15	1.278	1.662
			(35)30-20	1.451	1.841
			(35)30-25	1.440	2.531
Average k	**1.859**	**2.550**	**Average k**	**1.553**	**2.032**

The loading (up) case has a higher average stiffness value (single – 1.859 kN/mm, dual – 2.550 kN/mm) than the unloading case (down) (single – 1.553 kN/mm, dual – 2.032 kN/mm) for both configurations. This confirms the presence of hysteresis. The dual configuration has a higher stiffness (loading – 2.550 kN/mm, unloading – 2.032 kN/mm) than the single configuration (loading – 1.859 kN/mm, unloading – 1.553 kN/mm) for both the loading and unloading cases. This is expected since the dual configuration comprises of two tyres that are not much different from the single tyre in size and construction.

4.2. Averaged Load - Deflection Tests Results

Figure 28 shows the load vs displacement plot obtained from the load deflection tests at a speed of 0 km/h for the single tyre case. The plots for the other speeds for both single and dual tyres are presented in Appendix C1.

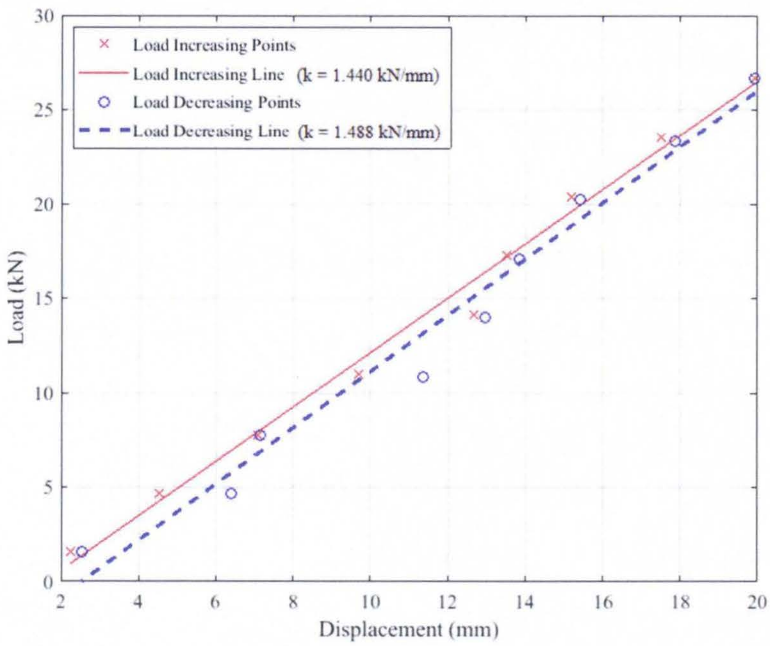

Figure 28: Load vs Displacement (Single Tyre at 0 km/h)

Figure 28 shows that the force vs displacement curve when increasing the load is above the curve when decreasing the load. This suggests hysteresis as expected. However, only the 0 km/h case load – deflection graphs clearly showed the loading line having values higher than the unloading line as expected. This is attributed to the speed of the test cases from which the graph data were derived. When rolling, the vertical load varies due to the runout of the tyres and rollers of the rig but when stationery, these variations are not present. This enabled the visibility of the load and deflection differences when loading and unloading at 0 km/h. When the load variations increased for the 15 km/h, 25 km/h and 35 km/h cases, the clarity was reduced and therefore the two loading and unloading lines are much closer together for these cases. In some of the load/unload cases, the unloading line was above the loading line and both clear load – deflection graphs for the 0 km/h cases show the loading line having a gradient (i.e. stiffness) lower than the unloading line gradient. This does not represent hysteresis theory and is also attributed to the disruption in the data collection by the presence of the load variations and system noise.

4.3. Model (k) vs Tests (k) Results

Table 10 shows the model vs tests stiffness (k) values obtained for each of the processed cases. The stiffness values presented in Table 9 were averaged with respect to their speeds to provide the values presented for the model.

Table 10: Model (k) vs Tests (k) Results

		Tests		**Model**	
		Singles	**Duals**	**Singles**	**Duals**
Step Direction	**Speed (km/h)**	**k (kN/mm)**	**k (kN/mm)**	**k (kN/mm)**	**k (kN/mm)**
Up	**0**	1.440	1.855	1.859	2.550
Down	**0**	1.488	1.880	1.691	2.221
	15	1.580	1.848	1.495	1.817
	25	1.515	1.789	1.544	2.113
	35	1.535	1.823	1.411	1.883

Both the tests and the model highlight that the dual configuration has a higher stiffness than the single configuration for both loading and unloading. However, unlike the tests as shown in the plots, the loading stiffness is higher than the unloading for all the model-based results as expected. This validates the comment on the load variations and noise affecting the values obtained from the load – deflection tests.

According to the model, at 0 km/h the dual configuration has a higher percentage difference (14.83%) between the loading stiffness and the unloading stiffness than the single configuration (9.90%). The area between the loading line and the unloading line represents the energy dissipated and this is directly proportional to the damping force (Fancher *et al.*, 1980). Therefore, the dual tyres experience a higher damping force.

4.4. Characteristic Deflection (β) Results

Table 11 shows the average characteristic deflection (β) values obtained for each of the processed cases.

Table 11: Characteristic Deflection (β) Results

Up			Down		
	Singles	Duals		Singles	Duals
(km/h) kN	β (mm)	β (mm)	(km/h) kN	β (mm)	β (mm)
(0)10-15	0.00601	0.00508	(0)10-3	0.07202	0.07162
(0)10-20	0.04476	0.04347	(0)10-5	0.03981	0.04728
(0)20-25	0.00881	0.01170	(0)20-10	0.02300	0.02921
(0)20-30	0.04101	0.05854	(0)20-15	0.01929	0.01758
(0)30-35	0.00979	0.00977	(0)30-20	0.02297	0.02707
(0)30-40	0.03382	0.04552	(0)30-25	0.00969	0.00975
			(15)20-10	0.02632	0.03733
			(15)20-15	0.01727	0.02436
			(15)30-20	0.02392	0.02866
			(15)30-25	0.00844	0.01010
			(25)20-10	0.02200	0.01206
			(25)20-15	0.01425	0.01305
			(25)30-20	0.02448	0.02648
			(25)30-25	0.00778	0.00994
			(35)20-10	0.02862	0.11015
			(35)20-15	0.02633	0.01769
			(35)30-20	0.02495	0.03001
			(35)30-25	0.01169	0.01340
Average β (mm)	**0.02403**	**0.02901**	**Average β (mm)**	**0.02349**	**0.02976**

When loading β = 0.02403 mm (single), β = 0.02901 mm (dual) and when unloading β = 0.02349 mm (single), β = 0.02976 mm (dual). β is a measure of the rate at which the response transitions into the boundary of the force envelop (i.e. straight-line portion. See Figure 30)

(Fancher *et al.*, 1980). Apart from the stiffness values, β also influences the amount of energy dissipated. According to the definition of β by Fancher *et al.* (1980), a higher β value results in a smaller area between the loading and unloading lines therefore such cases experience less damping force.

4.5. Model Fit Results

Figure 29 shows the model fit achieved during the processing of a 10 kN step load case for the dual tyre configuration at a speed of 0 km/h. Fits for the other test cases are presented in Appendix C2.

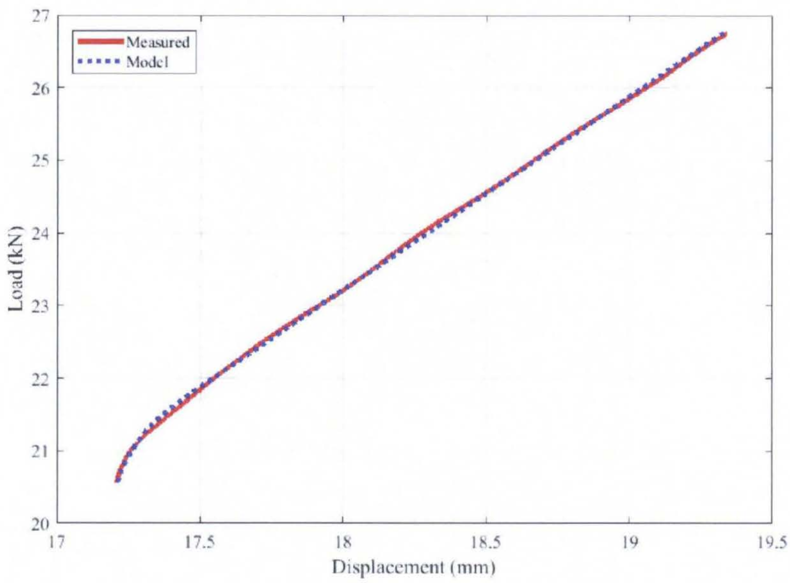

Figure 29: Load vs Displacement Fit (Dual Tyre | 30 kN – 40 kN at 0 km/h)

The model fit results shown in Figures 29 and Appendix C2 are all good. This confirms the ability of the proposed model to represent the force vs displacement relationship of tyres. The model fit plots for the negative step load cases show an initially steep portion of the force vs displacement line (right end of the line) that is much larger than that present for the fit plots for positive step load cases (left end of the line) which do not have the steep portion at all in some cases. The negative step load cases do not face the resistance faced by the positive load cases because of the tyre stiffness. The hydraulic cylinder extension is opposed by the force generated by the tyre deflection and tyre stiffness based on Hooke's law whereas the retraction is not opposed but supported by the release of potential energy by the tyre. Therefore, the load changes are initially faster than the deflection changes for the negative step load cases thus resulting in an initial steep section of the line.

The measured responses for the positive step load cases have more fluctuation (i.e. less close to being straight). This is attributed to a less smooth displacement response that resulted from the double integration of acceleration values with load variations when rolling and noise. This is more noticeable for the positive step load causes because the magnitude of the acceleration spike is less due to the resistance from the tyre previously mentioned. The amount of load variation and noise remained the same regardless of whether the step was negative or positive, but the magnitude of the acceleration spike increased when the step was negative. This is attributed to the potential energy storage of the tyres. Therefore, the load variation and noise affect the resulting displacement values more since the ratio of load variation and noise magnitude to acceleration spike magnitude is higher. In the fit plots, the measured response shows a transition into a straight line. The response's transition into a straight line indicates the characteristic deflection (β). The values summarised in Table 11 confirm the presence of a characteristic length (β) for the tyres.

The exact quantification of the hysteresis damping could not be accomplished due to the difficulty in determining the amount of frictional damping. Figure 30 below illustrates the difficulty.

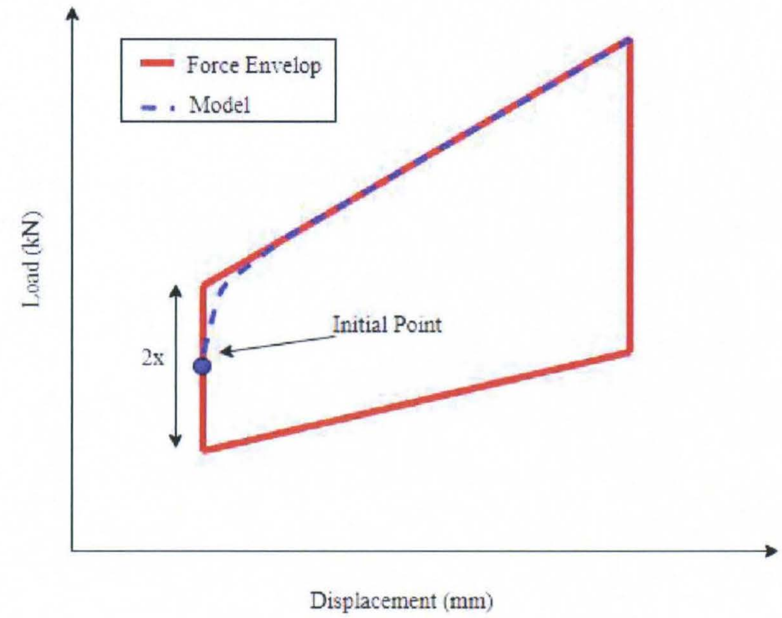

Figure 30: Force Envelop

The unknown value x represents the coulomb frictional damping. Since this value was unknown, it was not possible to determine how much friction the loading had overcome when the step loads were applied. Therefore, it was not possible to calculate the area enclosed by the force envelop to determine the hysteretic damping.

A large amount of noise was observed from the laser displacement sensor, accelerometer and load cell. Since the rig is believed to be sufficiently grounded, the noise experienced is attributed to the vibrations experienced and propagated through the rig when it is operation. This view is justified by the increase in the amplitude of the noise as speed increased. The presence of the noise and load variations affected the repeatability of the testing particularly the load deflection tests conducted at non-zero speeds. The repeatability of the testing was also affected by the inability to apply an exact and repeatable load using the hydraulic cylinder. Therefore, for the three tests conducted for each test case, the same set point load produced different actual loads. Although the overall repeatability of the results is satisfactory, these effects of the noise and hydraulic cylinder must be considered when analysing the results obtained from the testing.

Other issues encountered during the research were: the rig is rated to a limit of 45 kN and a speed of 35 km/h, the load control feedback loop resulted in the actual load applied being different to the load input into the rig control program and the manual override method is not repeatable therefore accurate calibration was not possible (i.e. the same input value produces different load values which are close but not equal). Although the research yielded satisfactory results, dealing with these issues will improve the results.

5. CONCLUSIONS

The stiffness of single and dual truck tyres was characterised. The following conclusions were made:

- The loading case has a higher average stiffness value (single – 1.859 kN/mm, dual – 2.550 kN/mm) than the unloading case (single – 1.553 kN/mm, dual – 2.032 kN/mm) for both configurations (i.e. tyres exhibit hysteresis).
- The dual configuration has a higher stiffness (loading – 2.550 kN/mm, unloading – 2.032 kN/mm) than the single configuration (loading – 1.859 kN/mm, unloading – 1.553 kN/mm).
- The hysteresis in the single and dual truck tyres was observed. A model was proposed to characterise the hysteresis. An important parameter of the model is the characteristic deflection, which captures the spatial rate with which the tyre transitions into the upper envelop of the force versus deflection curve when loading (β = 0.02403 mm (single), β = 0.02901 mm (dual)) and the lower envelop when unloading (β = 0.02349 mm (single), β = 0.02976 mm (dual)).

6. REFERENCES

Bin, L. & Xiaobo, Y., 2014. *In-Plane Rigid Ring-Based Tire Model:Parameter Identification, Sensitivity Analyses and Effect on Ride Comfort.* s.l., ASME.

Dugoff, H., Fancher, P. & Segel, L., 1969. *Tire Performance Characteristics Affecting Vehicle Response to Steering and Braking Control Inputs,* Michigan: The University of Michigan.

Els, P., Theron, N. & Thoresson, M., 2007. *Ride Comfort and Handling Compromise for Off-road Vehicles,* Pretoria: University of Pretoria.

Fancher, P., Ervin, R., MacAdam, C. & Winkler, C., 1980. *Measurement and Representation of the Mechanical Properties of Truck Leaf Springs,* Pennsylvania: Society of Automotive Engineers, Inc..

Geng, Z., Popov, A. & Cole, D., 2007. Measurement, identification and modelling of damping in pneumatic tyres. *International Journal of Mechanical Sciences,* Volume 49, pp. 1077-1094.

Gipser & Hofmann, 2018. *FTire - Flexible Structure Tire Model,* Munich: Cosin Scientific Software.

Gipser, M., 2007. FTire – The Tire Simulation Model for All Applications Related to Vehicle Dynamics. *Vehicle System Dynamics,* 45(1), pp. 139-151.

Gisper, M., 2015. *The FTire Tire Model Family,* Esslingen: Esslingen University.

Keyence, 2015. *CMOS Multi-Function Analog Sensor IL Series - Instruction Manual,* Japan: Keyence Corporation.

Lines, J. & Young, A., 1989. A Machine for Measuring the Suspension Characteristics of Agricultural Tyres. *Journal of Terramechanics,* 26(3), pp. 201-210.

Malzahn, Y. & Kienhöfer, F., 2014. *The Effect of Wheel Configuration on Vehicle Component Temperatures.* San Luis, 13th International Symposium on Heavy Vehicle Transport Technology.

Meggitt, n.d. *Model 7290E Variable Capacitance Accelerometer,* San Juan Capistrano: Endevco Corporation.

Pacejka, H., 1981. Analysis of Tire Properties. In: S. Clark, ed. *Mechanics of Pneumatic Tires.* Michigan: U.S Department of Transportation, pp. 727-887.

Pacejka, H., 2012. *Tire and Vehicle Dynamics.* s.l.:Elsevier Ltd.

Sayers, M. & Riley, S., 1996. *Modelling Assumption for Realistic Multibody Simulations of the Yaw and Roll Behavior of Heavy Trucks,* Detroit: SAE International.

Segel, L., Gillespie, T., Schneider, L. & Campell, K., 1981. *State of the Knowledge Review: Relationship of Truck Ride Vibration to Highway Safety,* Michigan: Highway Safety Research Institute, The University of Michigan.

Spivey, C., 2007. *Analysis of Ride Quality of Tractor Semi-Trailers,* s.l.: Clemson University - TigerPrints.

Taylor, R., Bashford, M. & Schrock, M., 2000. Methods for Measuring Vertical Tire Stiffness. *American Society of Agricultural Engineers,* 43(6), pp. 1415-1419.

Tounonen, A., Hartikainen, L., Petry, F. & Westermann, S., 2012. *Parameterization of In-plane Rigid Ring Tire Model from Instrumented Vehicle Measurements,* s.l.: Aalto University.

Wong, J., 2001. *Theory of Ground Vehicles.* 3rd ed. Ottawa: John Wiley & Sons.

Wu, G., Fan, G. & Guo, J., 2012. *Ride Comfort Evaluation for Road Vehicle Based on Rigid-flexible Coupling Multibody Dynamics,* Shanghai: Tongji University.

Zemic, 2016. *Calibration Certificate,* Shaanxi: Zemic.

APPENDICES

Appendix A1 – Mounting Part Drawing

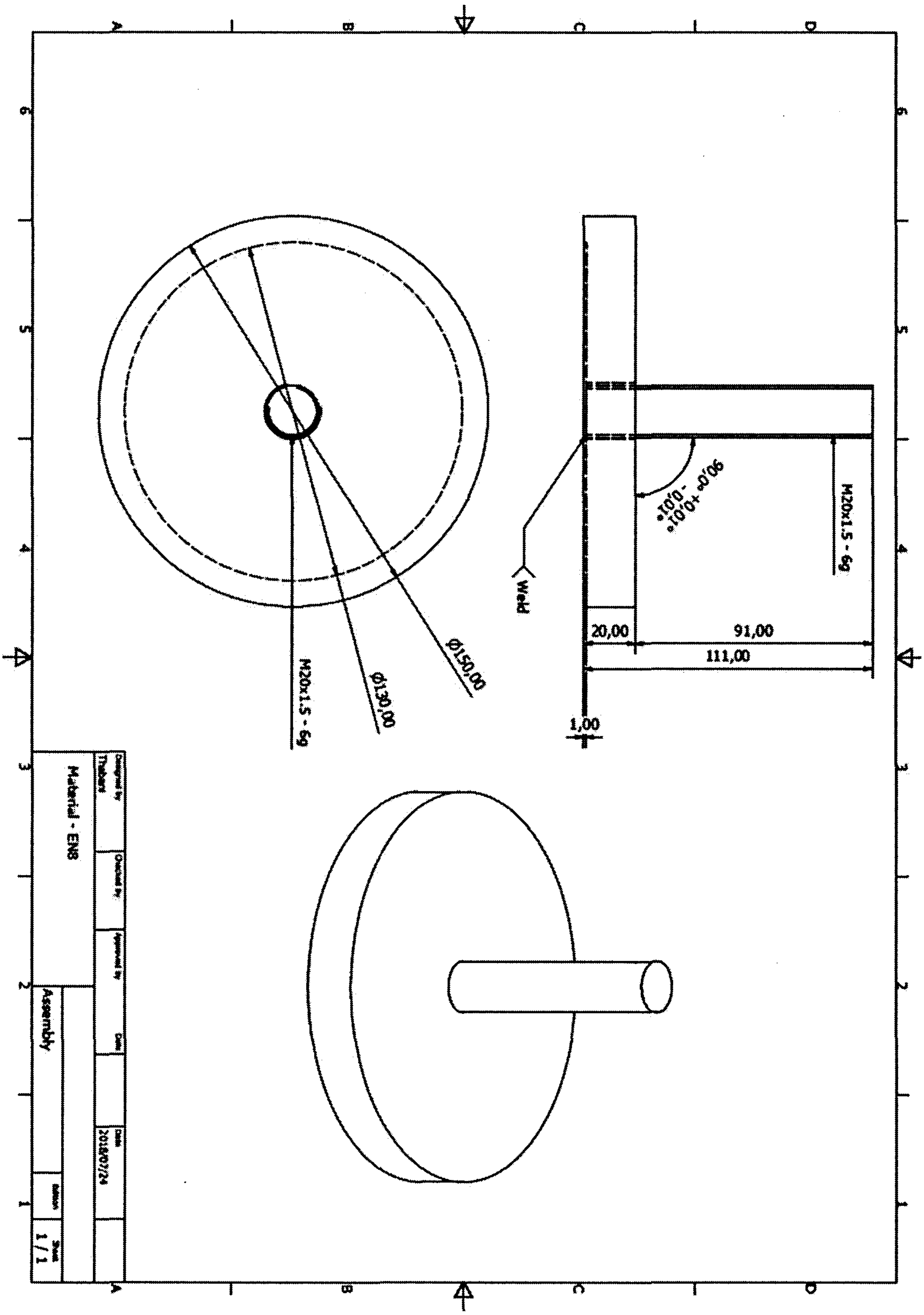

Appendix A2 – Load Deflection Tests LabView Program

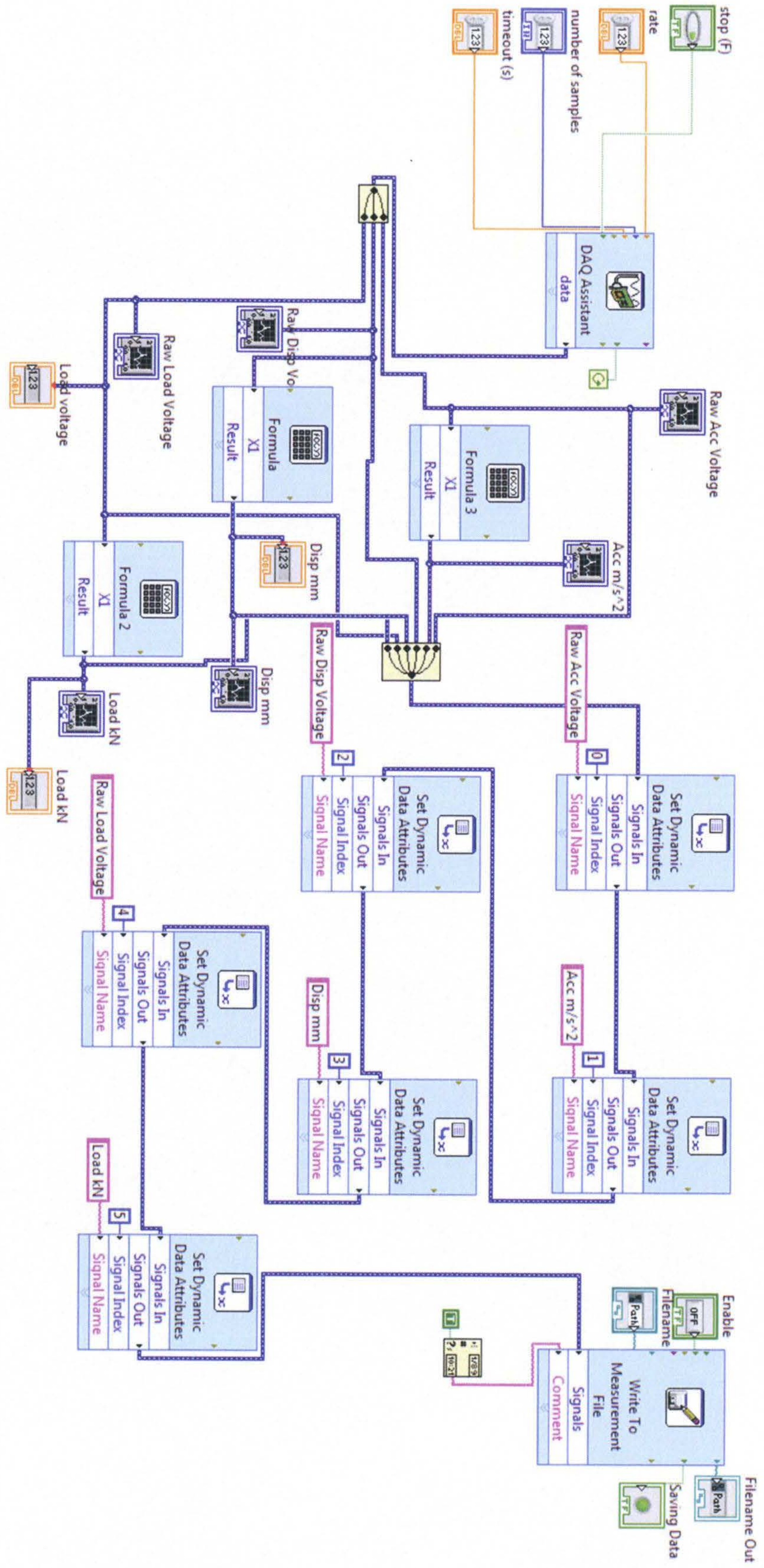

Appendix A3 – Step Load Tests LabView Program

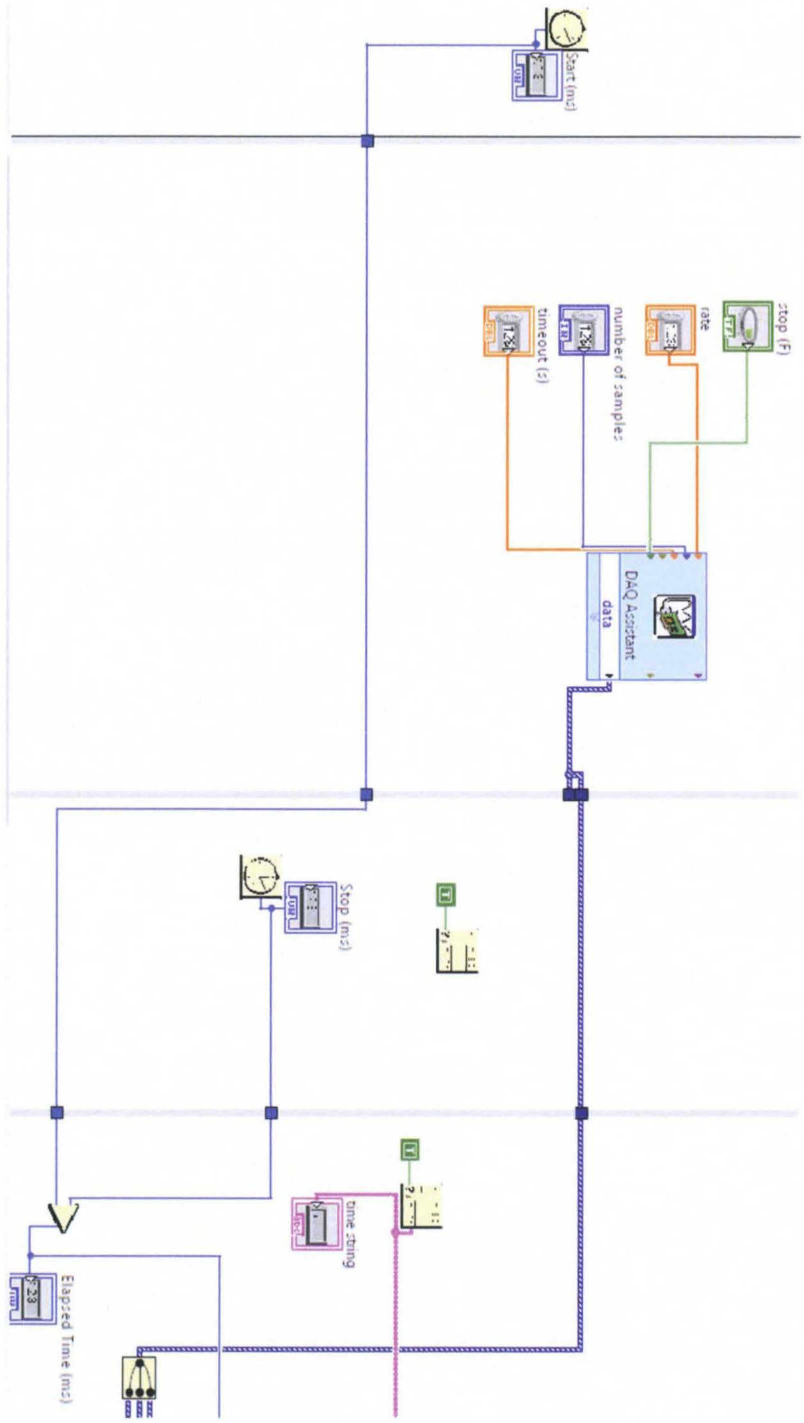

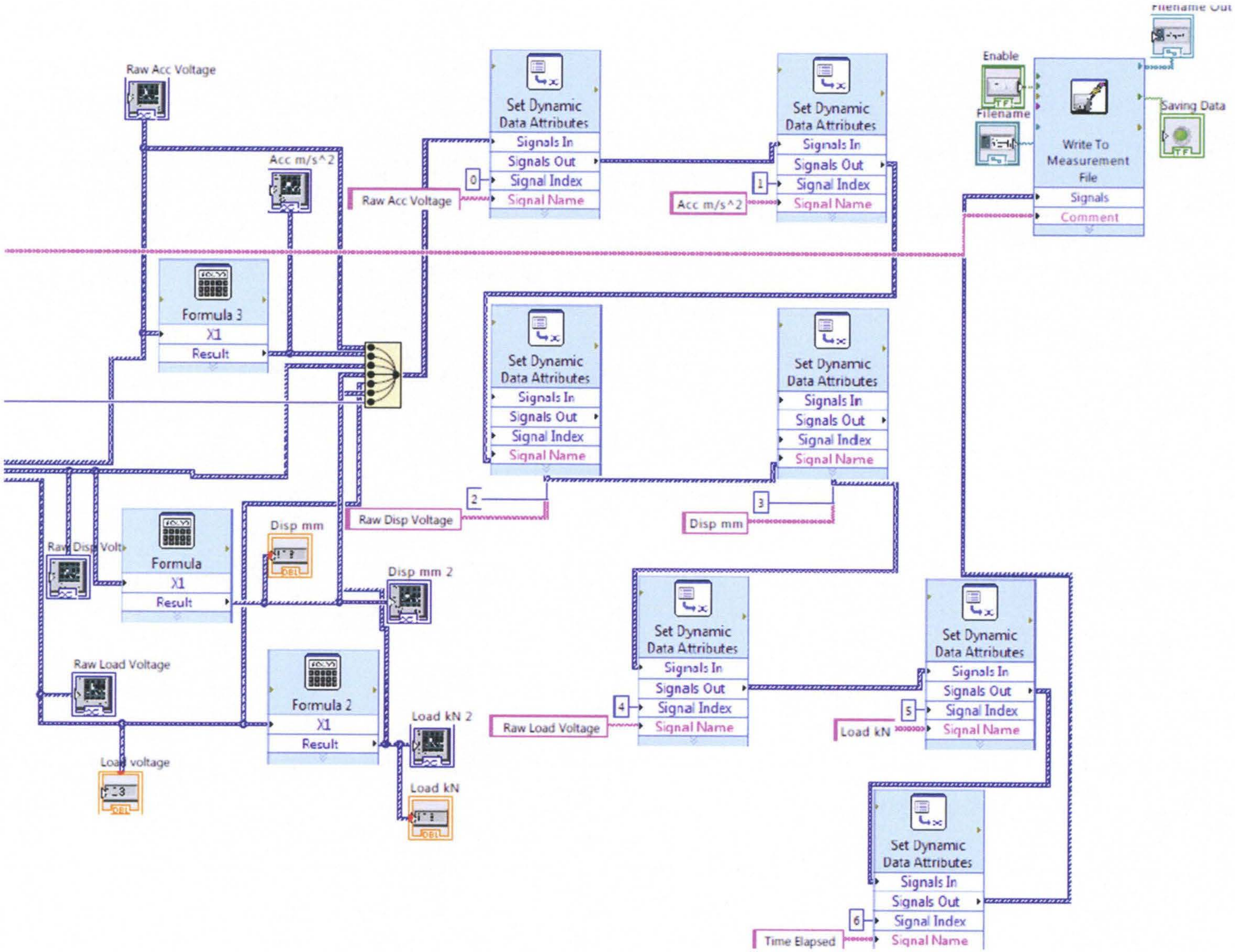

Raw Acc Voltage
Acc m/s^2
Set Dynamic Data Attributes
Signals In
Signals Out
Signal Index
Signal Name
0
Raw Acc Voltage
1
Acc m/s^2
Filename Out
Enable
Filename
Write To Measurement File
Signals
Comment
Saving Data
Formula 3
X1
Result
2
Raw Disp Voltage
3
Disp mm
Raw Disp Volt
Formula
Disp mm
Disp mm 2
Raw Load Voltage
Formula 2
Load kN 2
Load voltage
Load kN
4
Raw Load Voltage
5
Load kN
6
Time Elapsed

Appendix B1 – LabView Output Sample

LabVIEW Measurement								
Writer_Version	2							
Reader_Version	2							
Separator	Tab							
Decimal_Separator	.							
Multi_Headings	No							
X_Columns	One							
Time_Pref	Relative							
Operator	Wits-User							
Date	########							
Time	06:04:45.0332875251770019531							
End_of_Header								
Notes	X values guaranteed valid only for Raw Acc Voltage							
Channels	7							
Samples	150000	150000	150000	150000	150000	150000	1	
Date	########	########	########	########	########	########	########	
Time	06:04:45.0332875251770019531	06:04:45.0332875251770019531	06:04:45.0332875251770019531	06:04:45.0332875251770019531	06:04:45.0332875251770019531	06:04:45.0332875251770019531	06:04:45.0332875251770019531	
Y_Unit_Label	Volts	Volts	Volts	Volts	Volts	Volts		
X_Dimension	Time	Time	Time	Time	Time	Time	Time	
X0	0.0000000000000000E+0	0.0000000000000000E+0	0.0000000000000000E+0	0.0000000000000000E+0	0.0000000000000000E+0	0.0000000000000000E+0	0.0000000000000000E+0	
Delta_X	0.000100	0.000100	0.000100	0.000100	0.000100	0.000100	1.000000	
End_of_Header								
X_Value	Raw Acc Voltage	Acc m/s^2	Raw Disp Voltage	Disp mm	Raw Load Voltage	Load kN	Time Elapsed	Comment
0.000000	3.489576	0.029074	0.463741	661.529383	0.010404	29.632493	15144.000000	06:04:45
0.000100	3.490187	0.035202	0.463741	661.529383	0.010252	30.006036		
0.000200	3.486983	0.003032	0.463741	661.529383	0.010557	29.258949		
0.000300	3.489271	0.026011	0.463436	661.504115	0.010404	29.632493		
0.000400	3.487136	0.004564	0.463589	661.516749	0.010099	30.379580		
0.000500	3.490949	0.042862	0.463284	661.491481	0.010099	30.379580		
0.000600	3.488051	0.013755	0.463436	661.504115	0.010099	30.379580		
0.000700	3.489881	0.032138	0.463436	661.504115	0.010252	30.006036		
0.000800	3.487593	0.009159	0.463284	661.491481	0.010099	30.379580		
0.000900	3.490644	0.039798	0.463131	661.478846	0.010252	30.006036		
0.001000	3.488356	0.016819	0.463284	661.491481	0.009947	30.753124		
0.001100	3.491102	0.044394	0.463131	661.478846	0.010404	29.632493		
0.001200	3.488814	0.021415	0.463741	661.529383	0.009947	30.753124		
0.001300	3.490797	0.041330	0.463131	661.478846	0.010252	30.006036		
0.001400	3.488356	0.016819	0.463284	661.491481	0.010404	29.632493		

0.001500	3.490949	0.042862	0.463284	661.491481	0.010252	30.006036	
0.001600	3.490187	0.035202	0.463131	661.478846	0.010404	29.632493	
0.001700	3.490339	0.036734	0.463284	661.491481	0.010099	30.379580	
0.001800	3.489881	0.032138	0.463131	661.478846	0.010099	30.379580	
0.001900	3.490797	0.041330	0.463131	661.478846	0.010252	30.006036	
0.002000	3.490187	0.035202	0.463436	661.504115	0.010252	30.006036	
0.002100	3.490949	0.042862	0.463436	661.504115	0.010099	30.379580	
0.002200	3.490339	0.036734	0.463436	661.504115	0.010099	30.379580	
0.002300	3.489119	0.024479	0.463284	661.491481	0.010404	29.632493	
0.002400	3.490187	0.035202	0.463131	661.478846	0.010404	29.632493	
0.002500	3.488203	0.015287	0.463284	661.491481	0.010252	30.006036	
0.002600	3.490644	0.039798	0.463284	661.491481	0.010099	30.379580	
0.002700	3.488356	0.016819	0.463589	661.516749	0.010099	30.379580	
0.002800	3.490339	0.036734	0.463284	661.491481	0.010099	30.379580	
0.002900	3.489576	0.029074	0.463589	661.516749	0.010252	30.006036	
0.003000	3.491102	0.044394	0.463589	661.516749	0.010252	30.006036	
0.003100	3.488661	0.019883	0.463284	661.491481	0.010252	30.006036	
0.003200	3.490034	0.033670	0.463284	661.491481	0.010252	30.006036	
0.003300	3.488966	0.022947	0.463436	661.504115	0.010099	30.379580	
0.003400	3.488966	0.022947	0.463131	661.478846	0.010099	30.379580	
0.003500	3.490949	0.042862	0.463131	661.478846	0.010252	30.006036	
0.003600	3.488966	0.022947	0.463284	661.491481	0.010404	29.632493	
0.003700	3.490187	0.035202	0.463436	661.504115	0.010252	30.006036	
0.003800	3.486983	0.003032	0.463131	661.478846	0.010252	30.006036	
0.003900	3.490339	0.036734	0.462826	661.453578	0.010404	29.632493	
0.004000	3.489271	0.026011	0.462979	661.466212	0.010099	30.379580	
0.004100	3.490034	0.033670	0.462979	661.466212	0.010099	30.379580	
0.004200	3.487593	0.009159	0.462979	661.466212	0.010252	30.006036	
0.004300	3.491712	0.050521	0.463131	661.478846	0.010099	30.379580	
0.004400	3.490492	0.038266	0.462979	661.466212	0.010099	30.379580	
0.004500	3.492017	0.053585	0.463131	661.478846	0.010252	30.006036	
0.004600	3.491560	0.048989	0.463284	661.491481	0.010404	29.632493	
0.004700	3.492017	0.053585	0.462979	661.466212	0.010404	29.632493	
0.004800	3.490949	0.042862	0.463131	661.478846	0.010557	29.258949	
0.004900	3.492933	0.062777	0.463131	661.478846	0.010099	30.379580	
0.005000	3.492627	0.059713	0.462979	661.466212	0.010099	30.379580	
0.005100	3.491712	0.050521	0.463131	661.478846	0.010252	30.006036	
0.005200	3.492322	0.056649	0.463284	661.491481	0.010252	30.006036	
0.005300	3.492475	0.058181	0.462979	661.466212	0.010099	30.379580	
0.005400	3.492933	0.062777	0.463131	661.478846	0.010557	29.258949	
0.005500	3.490339	0.036734	0.462826	661.453578	0.010099	30.379580	
0.005600	3.491102	0.044394	0.463589	661.516749	0.010252	30.006036	
0.005700	3.490034	0.033670	0.463131	661.478846	0.010557	29.258949	

0.005800	3.491712	0.050521	0.463436	661.504115	0.010252	30.006036	
0.005900	3.489119	0.024479	0.463436	661.504115	0.010252	30.006036	
0.006000	3.492322	0.056649	0.463741	661.529383	0.010557	29.258949	
0.006100	3.487441	0.007628	0.463131	661.478846	0.010404	29.632493	
0.006200	3.489271	0.026011	0.463284	661.491481	0.010404	29.632493	
0.006300	3.487441	0.007628	0.463284	661.491481	0.010252	30.006036	
0.006400	3.489424	0.027543	0.463436	661.504115	0.010252	30.006036	
0.006500	3.486983	0.003032	0.463436	661.504115	0.009947	30.753124	
0.006600	3.488356	0.016819	0.463131	661.478846	0.010404	29.632493	
0.006700	3.485915	0.007692	0.463436	661.504115	0.010099	30.379580	
0.006800	3.488356	0.016819	0.463284	661.491481	0.010099	30.379580	
0.006900	3.487746	0.010691	0.463284	661.491481	0.010099	30.379580	
0.007000	3.487441	0.007628	0.463284	661.491481	0.010252	30.006036	
0.007100	3.488814	0.021415	0.463284	661.491481	0.009947	30.753124	
0.007200	3.485610	0.010756	0.463131	661.478846	0.010099	30.379580	
0.007300	3.488661	0.019883	0.463436	661.504115	0.010099	30.379580	
0.007400	3.485305	0.013819	0.463589	661.516749	0.010404	29.632493	
0.007500	3.486983	0.003032	0.463284	661.491481	0.010252	30.006036	
0.007600	3.484085	0.026075	0.463436	661.504115	0.010404	29.632493	
0.007700	3.487593	0.009159	0.463284	661.491481	0.010099	30.379580	
0.007800	3.484542	0.021479	0.463284	661.491481	0.010252	30.006036	
0.007900	3.487288	0.006096	0.462826	661.453578	0.010099	30.379580	
0.008000	3.483322	0.033734	0.462979	661.466212	0.010099	30.379580	
0.008100	3.486068	0.006160	0.463131	661.478846	0.010404	29.632493	
0.008200	3.483932	0.027607	0.463131	661.478846	0.010404	29.632493	
0.008300	3.486830	0.001500	0.463131	661.478846	0.010404	29.632493	
0.008400	3.485000	0.016883	0.463131	661.478846	0.010252	30.006036	
0.008500	3.484847	0.018415	0.463284	661.491481	0.010252	30.006036	
0.008600	3.483932	0.027607	0.462826	661.453578	0.009794	31.126668	
0.008700	3.484390	0.023011	0.462826	661.453578	0.010099	30.379580	
0.008800	3.486220	0.004628	0.463131	661.478846	0.010252	30.006036	
0.008900	3.484542	0.021479	0.463284	661.491481	0.010252	30.006036	
0.009000	3.485915	0.007692	0.463436	661.504115	0.010099	30.379580	
0.009100	3.483932	0.027607	0.463589	661.516749	0.010404	29.632493	
0.009200	3.487288	0.006096	0.463284	661.491481	0.010404	29.632493	
0.009300	3.485305	0.013819	0.463284	661.491481	0.010557	29.258949	
0.009400	3.486983	0.003032	0.463436	661.504115	0.010404	29.632493	
0.009500	3.483779	0.029139	0.463436	661.504115	0.010557	29.258949	
0.009600	3.486068	0.006160	0.463589	661.516749	0.010557	29.258949	
0.009700	3.485457	0.012287	0.463131	661.478846	0.010099	30.379580	
0.009800	3.487593	0.009159	0.463284	661.491481	0.010252	30.006036	
0.009900	3.486068	0.006160	0.463436	661.504115	0.010099	30.379580	

Appendix B2 – Axle Load on Tyres Calculations

Single Axle

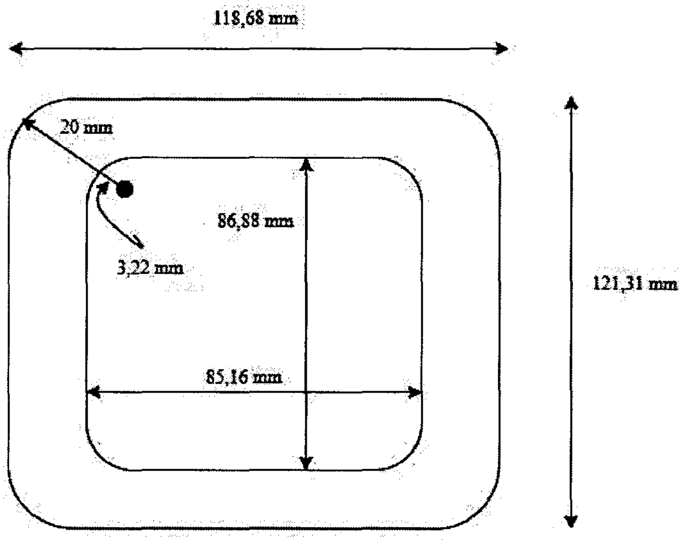

$$I = \frac{b_o h_o^3}{12} - \frac{b_i h_i^3}{12}$$

Where: I is the moment of inertia (to be used for deflection calculations) b_o is the length of the outer base, b_i is the length of the inner base, h_o is the outer height and h_i is the inner height. (Approximated as a rectangular tube).

$$I = \frac{0.1187(0.1213)^3}{12} - \frac{0.08688(0.08516)^3}{12}$$

$$I = 1.300 \times 10^{-5}\, m^4$$

$$A = b_o h_o - (4r_o^2 - \pi r_o^2) - [b_i h_i - (4r_i^2 - \pi r_i^2)]$$

Where: b_o is the length of the outer base, b_i is the length of the inner base, h_o is the outer height, h_i is the inner height, A is the cross-sectional area, r_o is the radius of the outer fillet and r_i is the radius of the inner fillet.

$$A = 0.1187(0.1213) - (4(0.02)^2 - \pi(0.02)^2) - [0.08516(0.08688) - (4(0.00322)^2 - \pi(0.00322)^2)]$$

$$A = 6.664 \times 10^{-3}\, m^2$$

$$V = A \times L$$

Where: V is the volume of the beam and L is the length of the beam.

$$V = 6.664 \times 10^{-3} \times 1.3$$

$$V = 8.663 \times 10^{-3}\ m^3$$

Assuming the beam covers the whole axle length and the density of steel:

$$W_B = V \times \rho \times g$$

Where: W_B is the weight of the beam, ρ is the density and g is the acceleration due to gravity.

$$W_B = 8.663 \times 10^{-3} \times 7700 \times 9.81$$

$$W_B = 654.4\ N$$

$$W_H = mg - W_B$$

Where: W_H is the weight of the wheel hub and m is the mass of the axle.

$$W_H = 290(9.81) - 654.4$$

$$W_H = 2191\ N$$

Taking the weight of the beam as a point load acting through the middle of the beam:

$$Axle\ Load\ on\ Tyre = W_H + W_{BWC}$$

Where: W_{BWC} is the load of the beam on the tyre.

$$Axle\ Load\ on\ Tyre = 2190.517 + \frac{650(654.4)}{1300}$$

$$Axle\ Load\ on\ Tyre = 2.518\ kN$$

Dual Axle

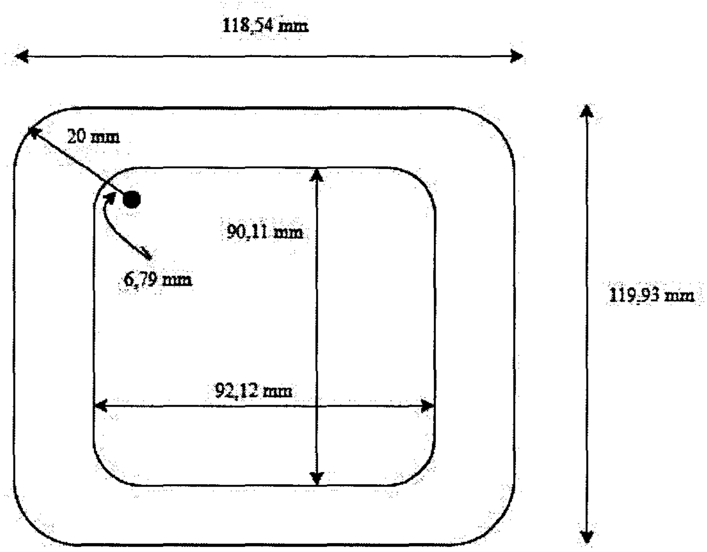

(Approximated as a rectangular tube).

$$I = \frac{b_o {h_o}^3}{12} - \frac{b_i {h_i}^3}{12}$$

$$I = \frac{0.1185(0.1199)^3}{12} - \frac{0.09212(0.09011)^3}{12}$$

$$I = 1.142 \times 10^{-5}\, m^4$$

$$A = b_o h_o - (4{r_o}^2 - \pi {r_o}^2) - [b_i h_i - (4{r_i}^2 - \pi {r_i}^2)]$$

$$A = 0.1185(0.1199) - (4(0.02)^2 - \pi(0.02)^2) - [0.09212(0.09011) - (4(0.00679)^2 - \pi(0.00679)^2)]$$

$$A = 5.612 \times 10^{-3}\, m^2$$

$$V = A \times L$$

$$V = 5.612 \times 10^{-3} \times 1.290$$

$$V = 7.239 \times 10^{-3}\, m^3$$

Assuming the beam covers the whole axle length and the density of steel:

$$W_B = V \times \rho \times g$$

$$W_B = 7.239 \times 10^{-3} \times 7700 \times 9.81$$

$$W_B = 546{,}8\ N$$

$$W_H = mg - W_B$$

$$W_H = 305(9.81) - 546.8$$

$$W_H = 2445\ N$$

Taking the weight of the beam as a point load acting through the middle of the beam:

$$Axle\ Load\ on\ Tyre = W_H + W_{BWC}$$

$$Axle\ Load\ on\ Tyre = 2445 + \frac{645(546.8)}{1290}$$

$$Axle\ Load\ on\ Tyre = 2.718\ kN$$

Appendix B3 – Deflection and Slope Calculations

For these calculations, the axles were approximated as simply supported and the maximum possible load (P = 45 kN) was used.

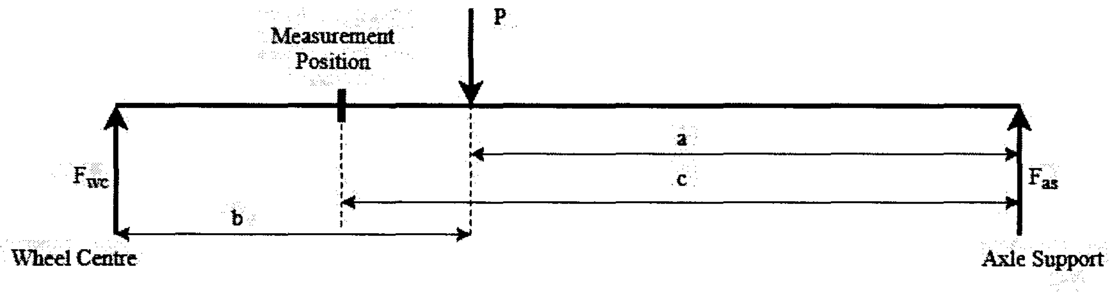

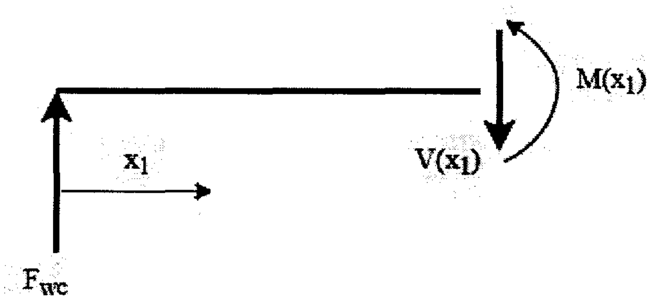

$$F_{wc} = \frac{Pa}{a+b}$$

Taking moments about the section point.

$$M(x_1) = \frac{Pa}{a+b} x_1$$

$$EI\frac{d^2v_1}{{dx_1}^2} = M(x_1)$$

$$EI\frac{dv_1}{dx_1} = \frac{Pa}{2(a+b)} {x_1}^2 + C_1$$

$$EIv_1 = \frac{Pa}{6(a+b)} {x_1}^3 + C_1x_1 + C_2$$

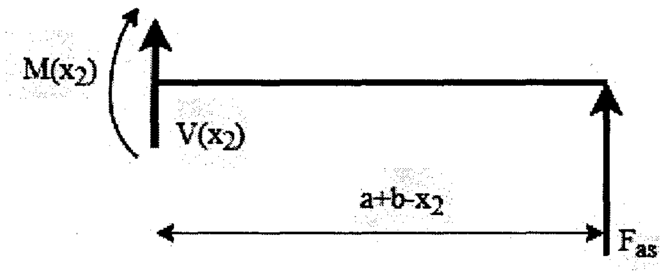

$$F_{as} = P - \frac{Pa}{a+b}$$

Taking moments about the section point:

$$M(x_2) = P\left(1 - \frac{a}{a+b}\right)(a + b - x_2)$$

$$EI\frac{d^2v_2}{dx_2{}^2} = M(x_2)$$

$$EI\frac{dv_2}{dx_2} = Pbx_2 - \frac{P}{2}\left(1 - \frac{a}{a+b}\right)x_2{}^2 + C_3$$

$$EIv_2 = \frac{Pbx_2{}^2}{2} - \frac{P}{6}\left(1 - \frac{a}{a+b}\right)x_2{}^3 + C_3x_2 + C_4$$

After applying the boundary conditions:

$$C_1 = \frac{Pb^2}{2} - \frac{2Pb(a+b)}{6} - \frac{Pb^3}{6(a+b)}$$

$$C_2 = 0$$

$$C_3 = -\frac{Pb(a+b)}{3} - \frac{Pb^3}{6(a+b)}$$

$$C_4 = \frac{Pb^3}{6}$$

Therefore:

$$\theta_1 = \frac{P}{EI}\left(\frac{ax_1{}^2}{2(a+b)} + \frac{b^2}{2} - \frac{b(a+b)}{3} - \frac{b^3}{6(a+b)}\right)$$

$$v_1 = \frac{P}{EI}\left(\frac{a{x_1}^3}{6(a+b)} + \left(\frac{b^2}{2} - \frac{b(a+b)}{3} - \frac{b^3}{6(a+b)}\right)x_1\right)$$

Single axle:

$$I = 1.300 \times 10^{-5}\, m^4$$

$$a = 0.875\, m$$

$$b = 0.425\, m$$

$$P = 45000\, N$$

$$x(measurement\ point) = 0.350\, m$$

Therefore:

$$v_1 = -5.448 \times 10^{-4}\, m$$

$$\theta_1 = -1.081 \times 10^{-3}\, rad$$

Dual axle:

$$I = 1.142 \times 10^{-5}\, m^4$$

$$a = 0.875\, m$$

$$b = 0.415\, m$$

$$P = 45000\, N$$

$$x(measurement\ point) = 0.405\, m$$

Therefore:

$$v_1 = -6.623 \times 10^{-4}\, m$$

$$\theta_1 = -9.049 \times 10^{-4}\, rad$$

At a load of 45 kN the deflection and slope values are negligible. The maximum loads and step loads are less than 45 kN therefore deflection and slope did not significantly affect the data obtained.

Appendix B4 – Rollers to Flat Ground Conversions Derivation

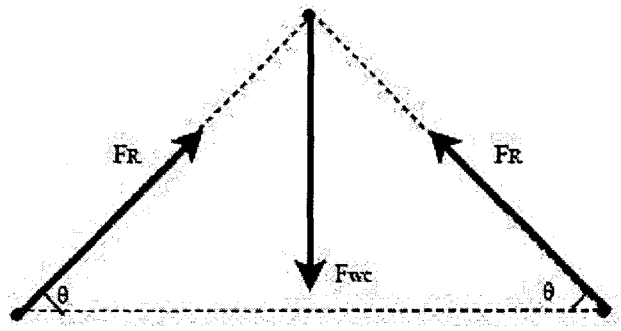

$$-F_{wc} + 2F_R \sin\theta = 0$$

$$F_R = \frac{F_{wc}}{2\sin\theta}$$

Where: F_R is the load experienced at the roller-tyre contact surface.

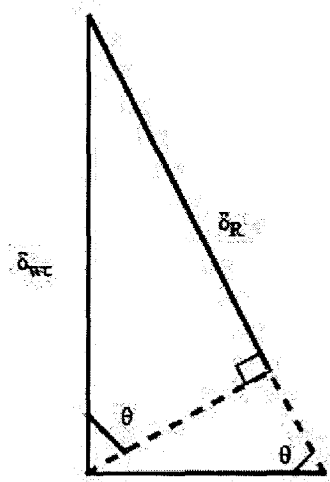

For the deflections expected, the change in θ is negligible therefore:

$$\delta_R \approx \delta_{wc} \sin\theta$$

Where: δ_R is the displacement experienced at the roller-tyre contact surface.

$$F_{wc} = k_{wc}\delta_{wc}$$

Where: k_{wc} is the stiffness value determined from the force and displacement values at the wheel centre.

$$k_{wc} = \frac{F_{wc}}{\delta_{wc}} = \frac{2\,F_R \sin\theta}{\frac{\delta_R}{\sin\theta}} = 2\,(\sin\theta)^2 \frac{F_R}{\delta_R} = 2\,(\sin\theta)^2 k_R$$

Where: k_R is the stiffness determined from the force and displacement values at the roller-tyre contact surface.

$$F_f = k_f \delta_f$$

Where: k_f is the stiffness determined from the force and displacement values on a flat surface. To determine the forces and displacements on a flat ground from those experienced at the roller-tyre contact surface, the curvature of the rollers must be considered. This is accomplished by Equation (a) (Pacejka, 1981).

$$k_f = k_R \left(\frac{R_r}{R_r + R_t}\right)^{-1/3} \qquad (a)$$

Where: R_r is the radius of the rollers and R_t is the unloaded radius of the tyre.

$$k_f = \frac{k_{wc}}{2\,(\sin\theta)^2} \left(\frac{R_r}{R_r + R_t}\right)^{-1/3}$$

$$\frac{F_f}{\delta_f} = \frac{1}{2\,(\sin\theta)^2} \left(\frac{R_r}{R_r + R_t}\right)^{-1/3} \frac{F_{wc}}{\delta_{wc}}$$

$$\delta_f = \delta_{wc} \sin\theta$$

$$F_f = \frac{F_{wc}}{2\sin\theta} \left(\frac{R_r}{R_r + R_t}\right)^{-1/3}$$

Single:

$$F_f = \frac{F_{wc}}{2\sin\theta} \left(\frac{133.5}{133.5 + 22.5 \times \frac{25.4}{2} + 0.65(385)}\right)^{-1/3}$$

$$F_f = \frac{F_{wc}}{1.168\sin\theta}$$

Dual:

$$F_f = \frac{F_{wc}}{2\sin\theta}\left(\frac{133.5}{133.5 + 22.5 \times \frac{25.4}{2} + 0.8(315)}\right)^{-1/3}$$

$$F_f = \frac{F_{wc}}{1.167\sin\theta}$$

The curvature factor was applied to the force values because on a curved surface, the tension force experienced in the tread band will influence the transmission of the force (Pacejka, 1981).

Appendix B5 – MATLAB code

Singles Input

```
%Step 1
clear
filename = 'Raw\Singles\DynamicS(0)30-20(1).xlsx';          %data file from LabView
[~,txt,~] = xlsread(filename);                               %read values obtained from tests
Time = str2double(txt(:,1));                                 %Time at which values are obtained

Accel = str2double(txt(:,3))*1000;                           %Acceleration values obtained and
change to mm
LDisp = str2double(txt(:,12));                               %Laser Transducer displacements
obtained
Loads = str2double(txt(:,13));                               %Load values obtained

Timestep = Time(2);                                          %timestep according to samples
taken and sample rate in Labview

%averages for replacement
AveAcc = mean(Accel(1:20000));                               %average before selected start
point for acceleration
AveLoadB = mean(Loads(1:20000));                             %average before selected start
point for Loads
AveLoadA = mean(Loads((length(Loads)-20000):length(Loads)));%average after selected start
point for Loads
AveLDispB = mean(LDisp(1:20000));                            %average before selected start
point for Laser displacements
AveLDispA = mean(LDisp((length(LDisp)-20000):length(LDisp)));%average after selected start
point for Laser displacements
Accel = Accel - AveAcc;                                      %zeroing the acceleration

%Step 2
%Replacement of values before start points and after end points
%%{
Loads(1:45102) = AveLoadB;
Loads(45498:length(Loads)) = AveLoadA;
Accel(1:45093) = 0;
%}

Velocity = cumtrapz(Time,Accel);            %Velocity

ADisp = cumtrapz(Time,Velocity);            %Accelerometer displacements

%Step 3
%%{
ADisp(45499:length(ADisp),1) = 2.9283;     %replacement after max/min
ADisp = movmean(ADisp,801);                %smoothing displacements
Loads = movmean(Loads,801);                %smoothing loads
%}

%%{
ADisp1 = ADisp*-(1300/950);                 %MP to WC conversion
ADisp2 = zeros(length(ADisp),1);
for count = 1:length(ADisp1)                %WC to F conversion
    sinT = (619.85583-ADisp1(count))/((((619.85583-ADisp1(count))^2)+(253^2))^(1/2));
    ADisp2(count) = ADisp1(count)*sinT;
end
FinalDisp = ADisp2 + AveLDispB;             %Absolute displacement
plot(Time,FinalDisp);
%}
```

Duals Input

```
%Step 1
clear
filename = 'Raw\Singles\DynamicD(0)30-20(1).xlsx';          %data file from LabView
[~,txt,~] = xlsread(filename);                              %read values obtained from tests
Time = str2double(txt(:,1));                                %Time at which values are obtained

Accel = str2double(txt(:,3))*1000;                          %Acceleration values obtained and
change to mm
LDisp = str2double(txt(:,12));                              %Laser Transducer displacements
obtained
Loads = str2double(txt(:,13));                              %Load values obtained

Timestep = Time(2);                                         %timestep according to samples
taken and sample rate in Labview

%averages for replacement
AveAcc = mean(Accel(1:20000));                              %average before selected start
point for acceleration
AveLoadB = mean(Loads(1:20000));                            %average before selected start
point for Loads
AveLoadA = mean(Loads((length(Loads)-20000):length(Loads)));%average after selected start
point for Loads
AveLDispB = mean(LDisp(1:20000));                           %average before selected start
point for Laser displacements
AveLDispA = mean(LDisp((length(LDisp)-20000):length(LDisp)));%average after selected start
point for Laser displacements
Accel = Accel - AveAcc;                                     %zeroing the acceleration

%Step 2
%Replacement of values before start points and after end points
%%{
Loads(1:45102) = AveLoadB;
Loads(45498:length(Loads)) = AveLoadA;
Accel(1:45093) = 0;
%}

Velocity = cumtrapz(Time,Accel);                %Velocity

ADisp = cumtrapz(Time,Velocity);                %Accelerometer displacements

%Step 3
%%{
ADisp(45499:length(ADisp),1) = 2.9283;         %replacement after max/min
ADisp = movmean(ADisp,801);                    %smoothing displacements
Loads = movmean(Loads,801);                    %smoothing loads
%}

%%{
ADisp1 = ADisp*-(1290/885);                     %MP to WC conversion
ADisp2 = zeros(length(ADisp),1);
for count = 1:length(ADisp1)                    %WC to F conversion
    sinT = (621.745577-ADisp1(count))/((((621.745577-ADisp1(count))^2)+(253^2))^(1/2));
    ADisp2(count) = ADisp1(count)*sinT;
end
FinalDisp = ADisp2 + AveLDispB;                 %Absolute Displacement
plot(Time,FinalDisp);
%}
```

Optimisation Function (Model)

```
function [out] = fun_beta(par,x,y,x0,y0)
k = par(1);                    %envelop stiffness
C = par(2);                    %envelop y-intercept
beta = par(3);                 %characteristic deflection
out = (y-y0)-(((k*x)+C)-y0).*(1-exp((-1*(abs(x-x0)))/beta)); %residual
```

Datafit (Optimisation of Model)

```
%isolate responce region
x = zeros(45899-44702+1,1);
x(1:(45899-44702+1)) = FinalDisp(44702:45899);
y = zeros(45899-44702+1,1);
y(1:(45899-44702+1)) = Loads(44702:45899);


% x is from FinalDisp, y is from Loads
N = ceil(length(x)*0.7);                                  %Data point roughly 70%
in
n1 = ceil(length(x)*0.2);                                 %Data point roughly 20%
in

x1 = x(1:N,1);                                            %Discard the last 30%
y1 = y(1:N,1);                                            %Discard the last 30%
x1a=x(n1:N,1);                                            %Take out just the
roughly straight line
y1a=y(n1:N,1);                                            %Take out just the
roughly straight line

plot(x1,y1,'bo',x1a,y1a,'yx')                             %Plot the experimental
points

options = optimset('LargeScale', 'off','Display','iter','Jacobian','off','MaxFunEvals', 250);
%optimisation settings

k0 = (y1(N)-y1(n1))/(x1(N)-x1(n1));                       %Best initial guess for
tyre stiffness
C0 = y1(n1)-k0*x1(n1);                                    %Best initial guess for
y-intercept
beta0 = 0.1;                                              %Best initial guess for
characteristic length
par0 = [k0 C0 beta0];

par = lsqnonlin('fun_beta', par0, [], [], options,x1,y1,x1(1),y1(1)); %Optimised solution
k = par(1);
C = par(2);
beta = par(3);

y2 = y1(1)+(((k*x1)+C)-y1(1)).*(1-exp((-1*(abs(x1-x1(1))))/beta));      %calculated force with
final beta
hold on
plot(x1,y2,'r.')                                          %Plot the fitted curve
disp(beta);
```

Write

```
%filename = 'Processed\Singles\PrcdDynS(35)30-25(3).xlsx';      %filename to save processed
data
filename = 'Processed\Duals\PrcdDynD(35)30-25(3).xlsx';         %filename to save processed
data
A = zeros(length(Time),10);                                     %initialise results matrix

A(:,1) = Time;                      %enter time data into results matrix
A(:,2) = LDisp;                     %enter laser transducer displacement data into
results matrix
A(:,3) = FinalDisp;                 %enter displacement data from accelerometer
integration into results matrix
A(:,4) = Loads;                     %enter loads data into results matrix
A(1:length(x),5) = x;               %enter response region accelerometer
displacement data into results matrix
A(1:length(y),6) = y;               %enter response region loads data into results
matrix
A(1:length(x1),7) = x1;             %enter limited version of x data into results
matrix
A(1:length(y1),8) = y1;             %enter limited version of y data into results
matrix
A(1:length(y2),9) = y2;             %enter optimised model loads data into results
matrix
A(1:length(par),10) = par;          %enter k,C and beta data into results matrix

xlswrite(filename,A)                %write to excel file
```

Appendix B6 – Dial Gauge Measurement

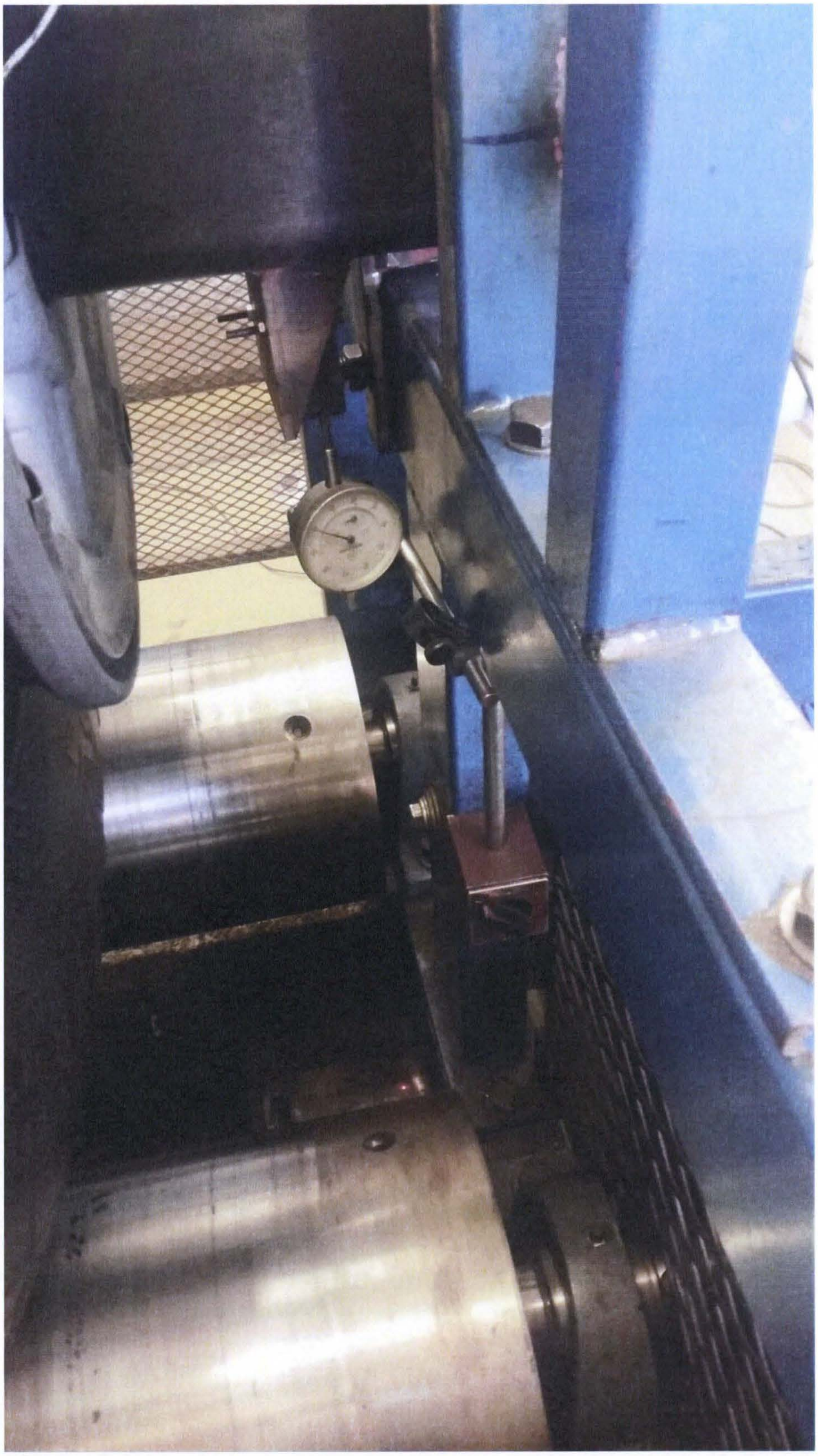

Dial Gauge Placement

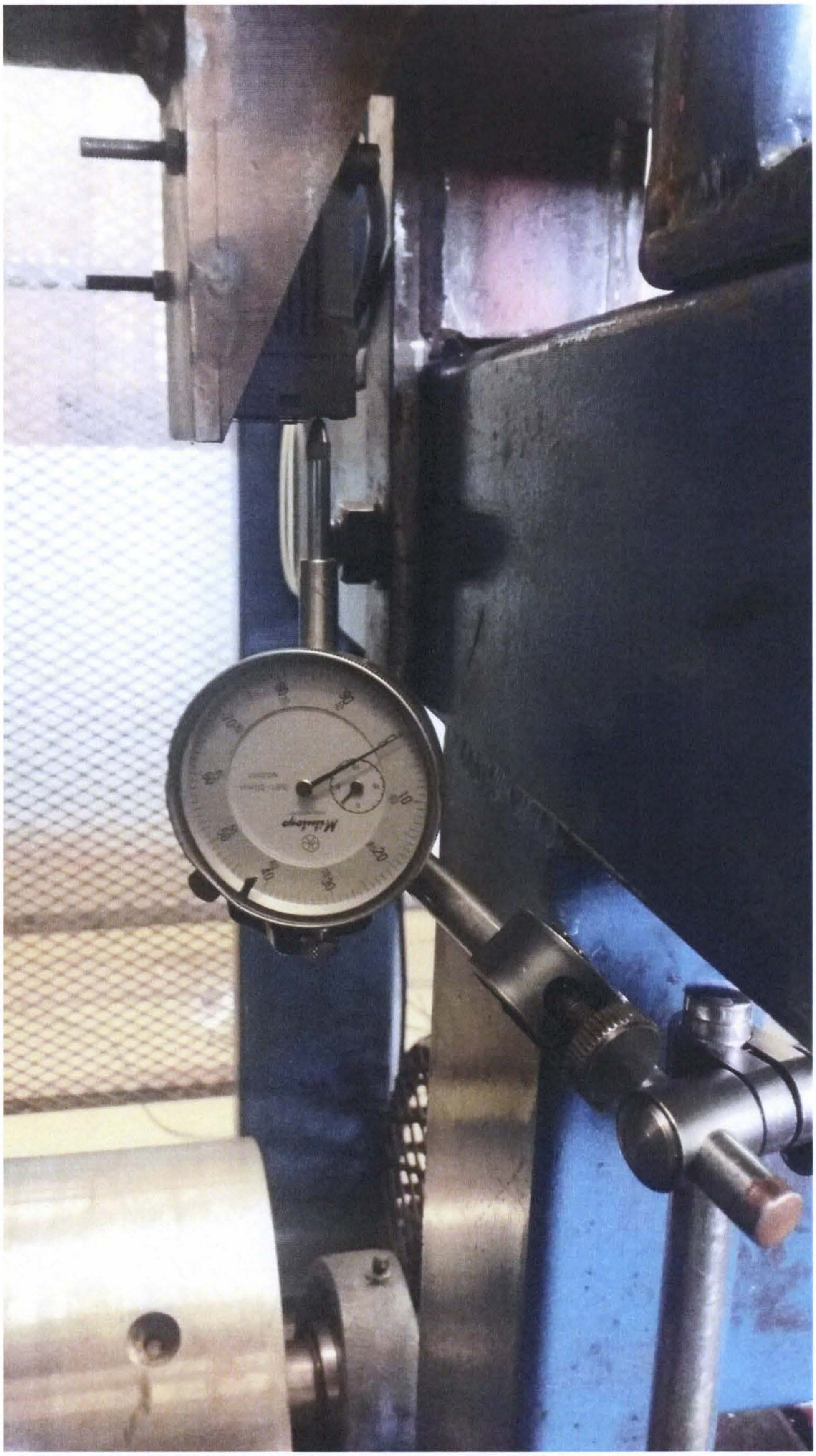

Dial Gauge Measurement

Appendix C1 – Averaged Load – Deflection Test Results

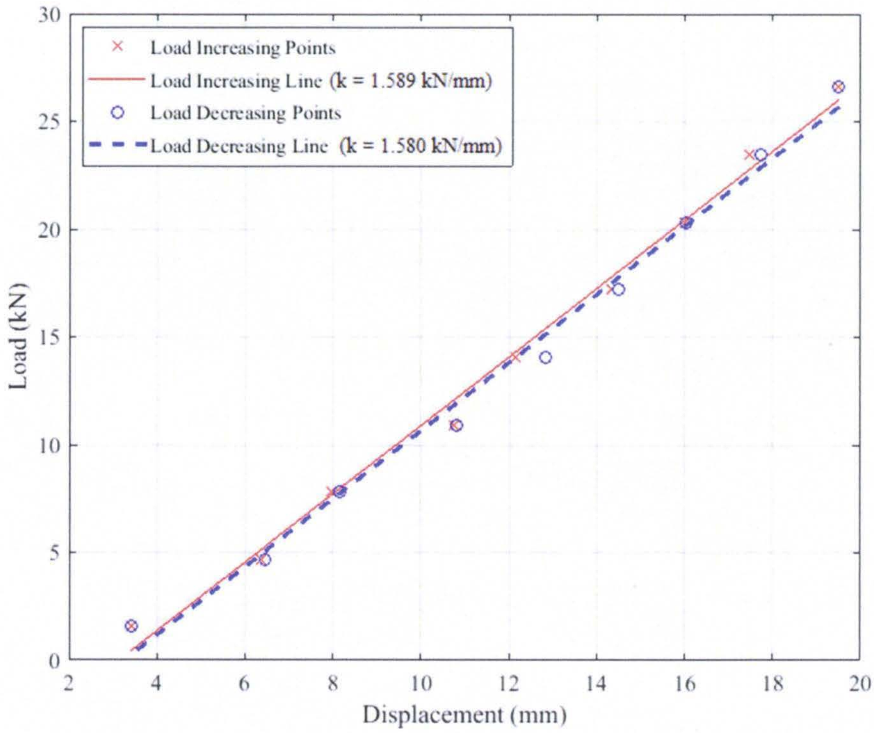

Load vs Displacement (Single Tyre at 15 km/h)

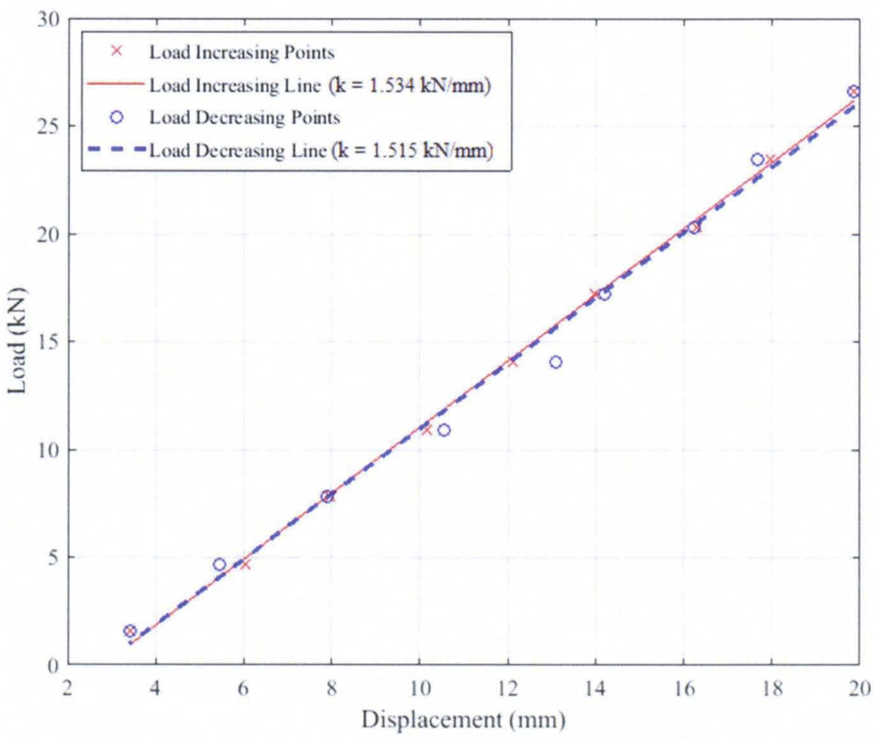

Load vs Displacement (Single Tyre at 25 km/h)

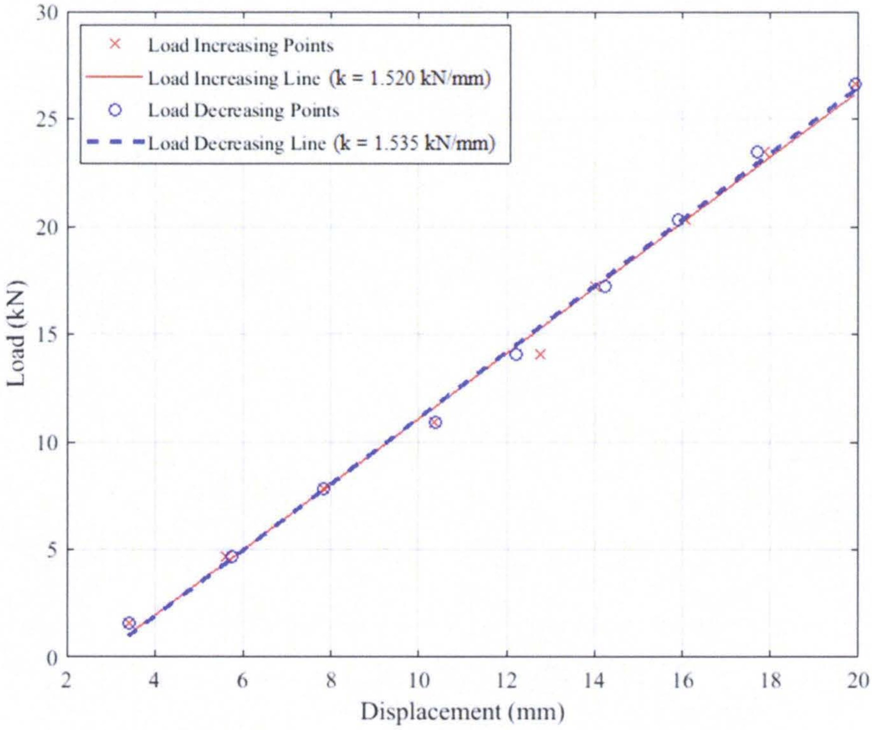

Load vs Displacement (Single Tyre at 35 km/h)

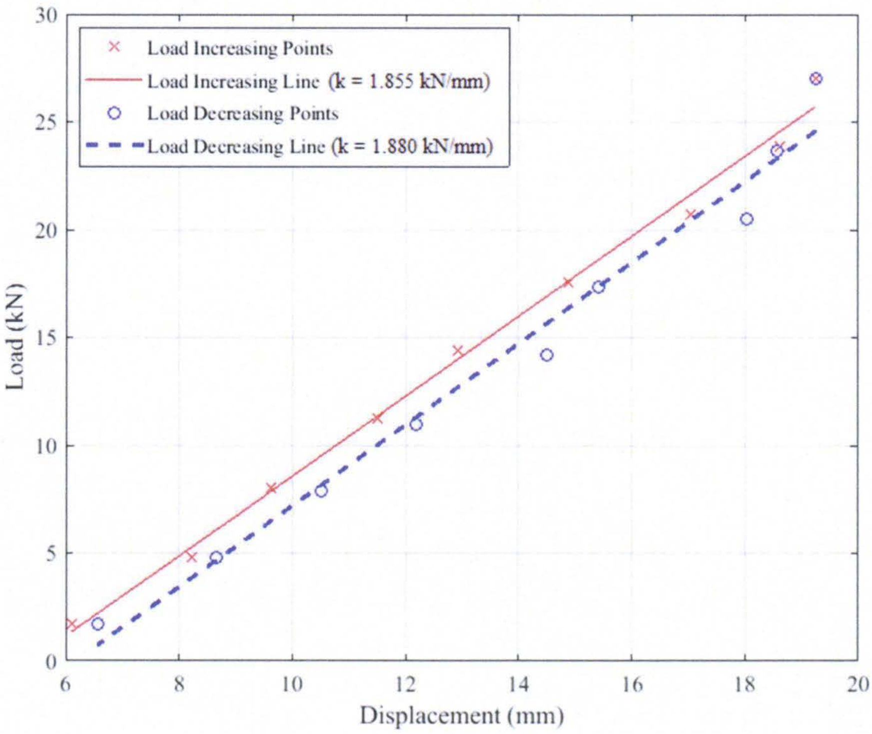

Load vs Displacement (Dual Tyre at 0 km/h)

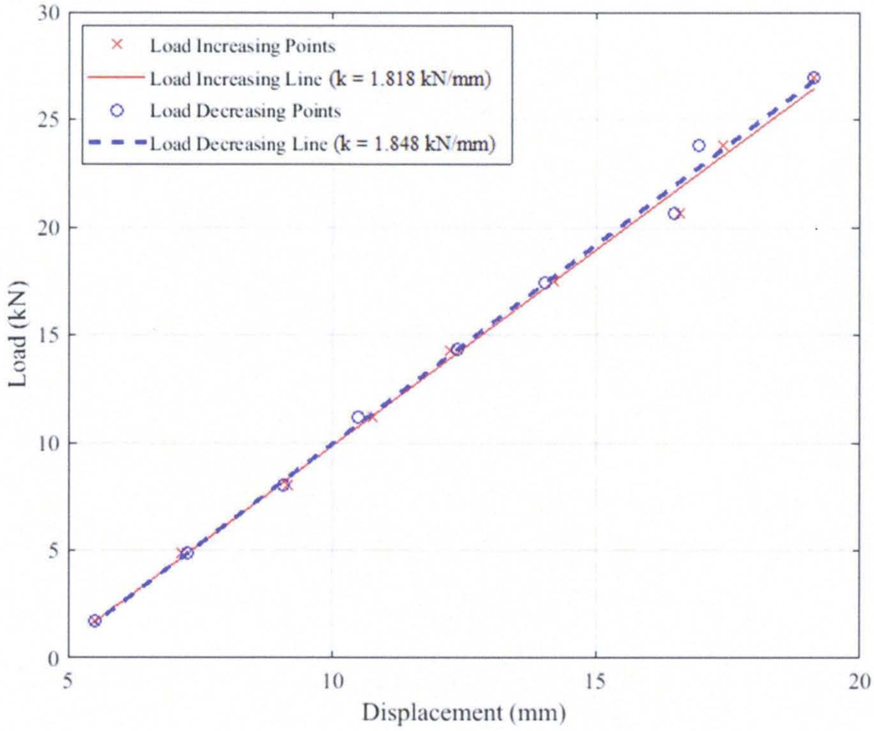

Load vs Displacement (Dual Tyre at 15 km/h)

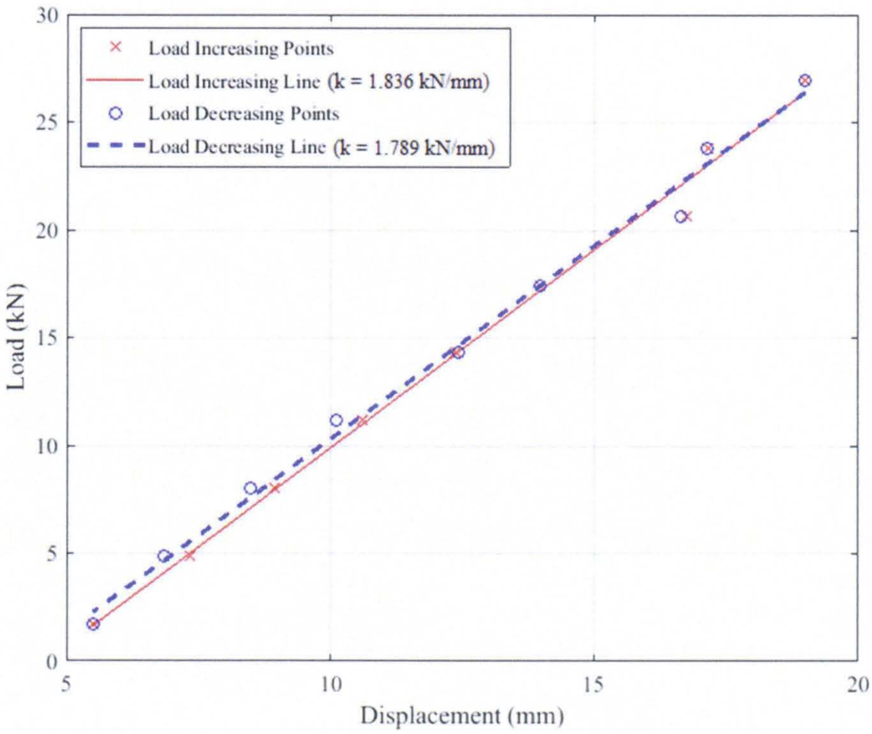

Load vs Displacement (Dual Tyre at 25 km/h)

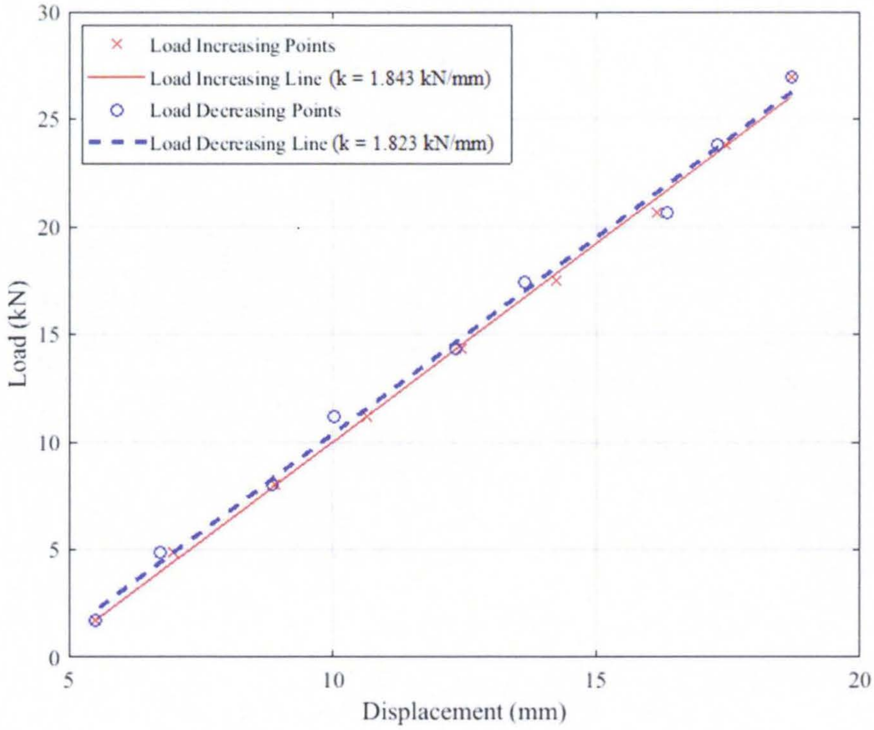

Load vs Displacement (Dual Tyre at 35 km/h)

Appendix C2 – Model Fit Results

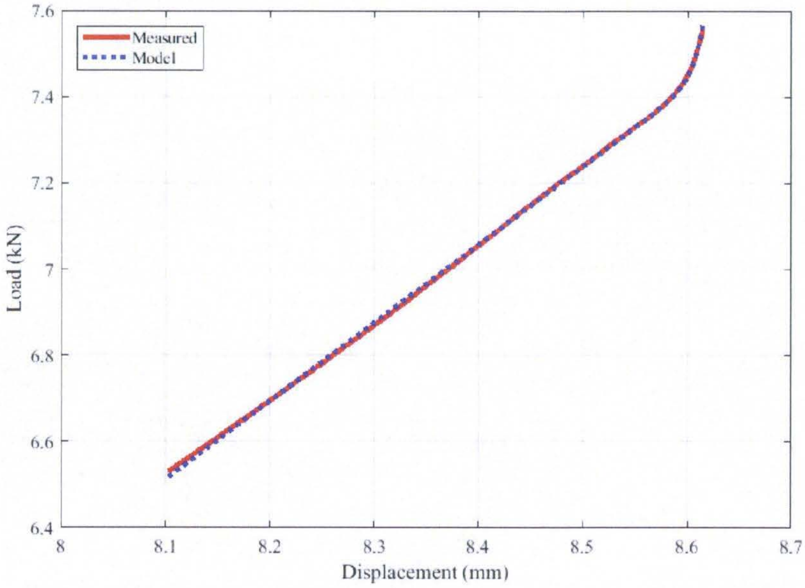

Load vs Displacement Fit (Single Tyre | 10 kN – 3 kN at 0 km/h)

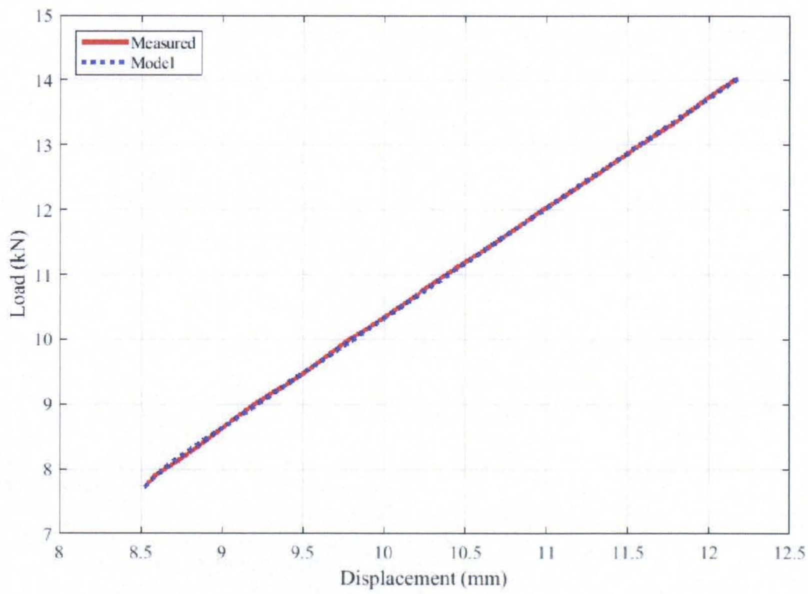

Load vs Displacement Fit (Single Tyre | 10 kN – 20 kN at 0 km/h)

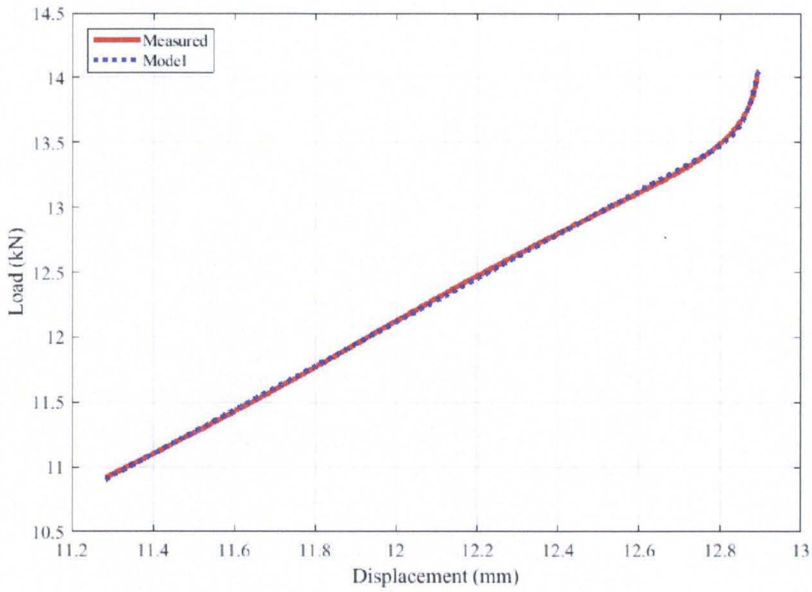

Load vs Displacement Fit (Single Tyre | 20 kN – 10 kN at 0 km/h)

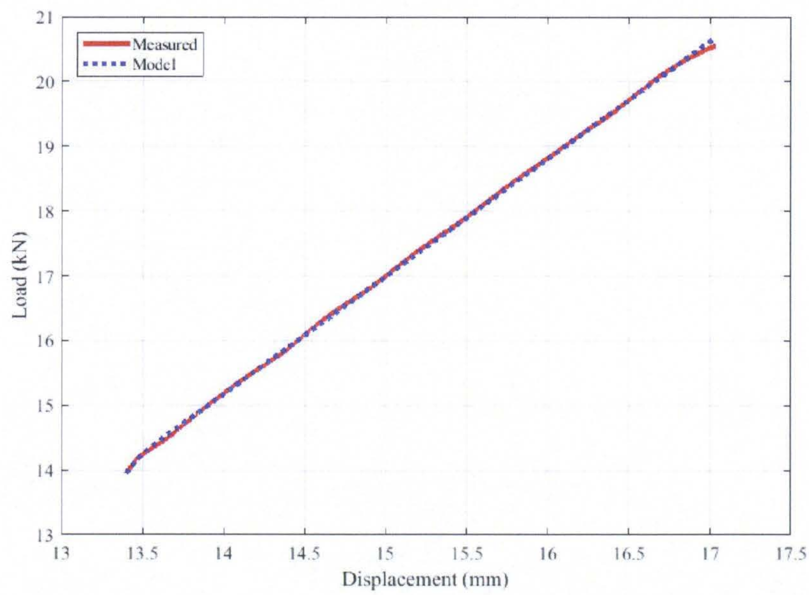

Load vs Displacement Fit (Single Tyre | 20 kN – 30 kN at 0 km/h)

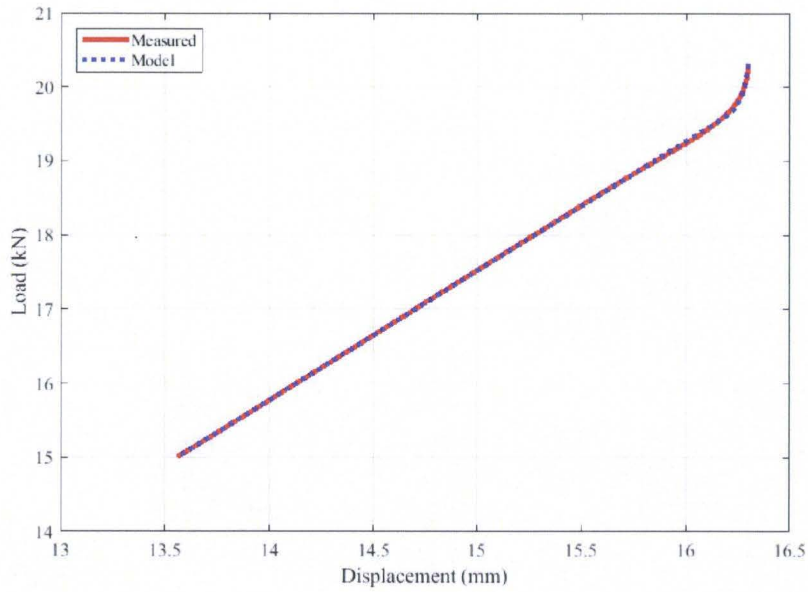

Load vs Displacement Fit (Single Tyre | 30 kN – 20 kN at 0 km/h)

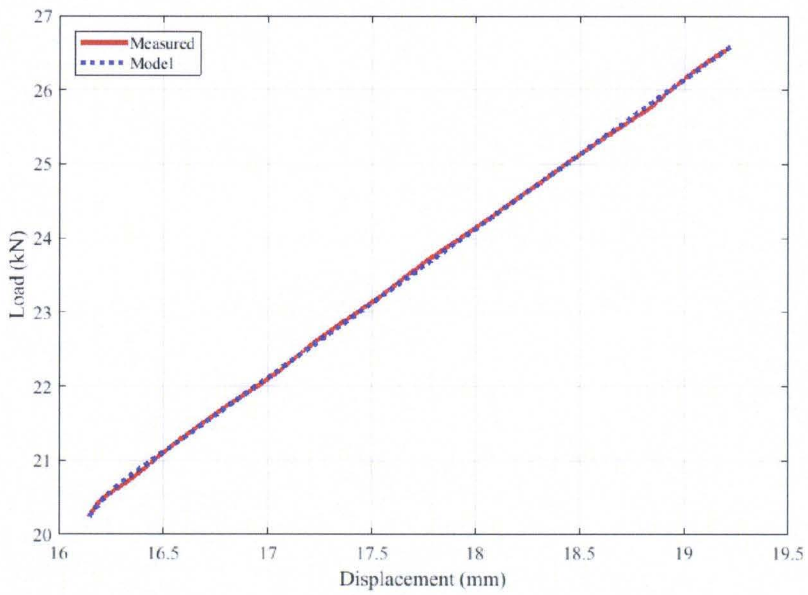

Load vs Displacement Fit (Single Tyre | 30 kN – 40 kN at 0 km/h)

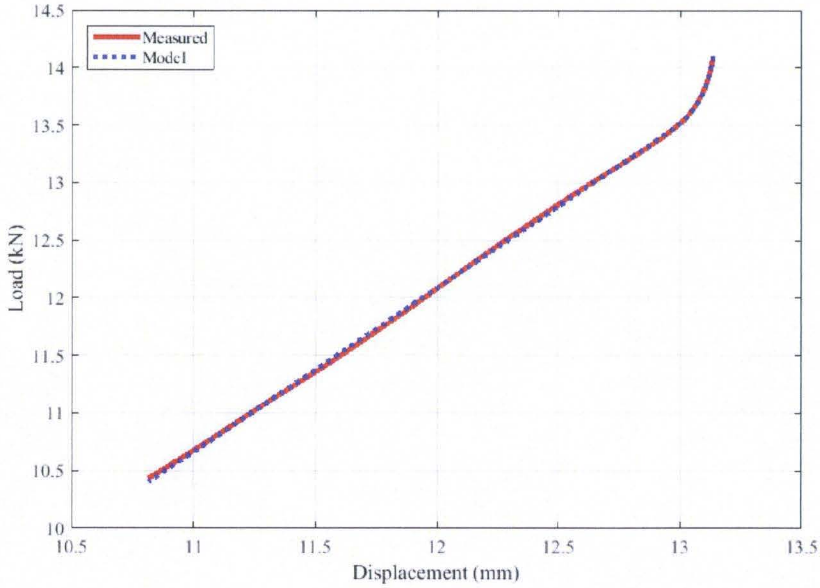

Load vs Displacement Fit (Single Tyre | 20 kN – 10 kN at 15 km/h)

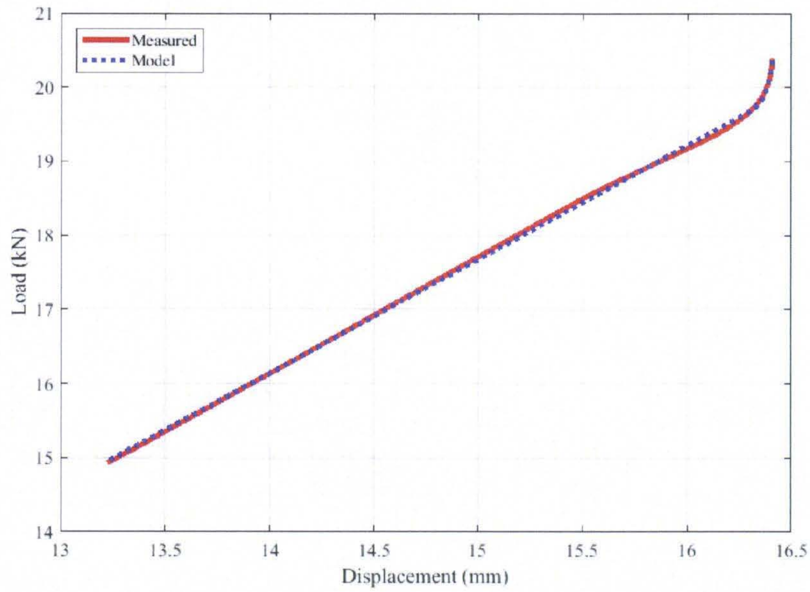

Load vs Displacement Fit (Single Tyre | 30 kN – 20 kN at 15 km/h)

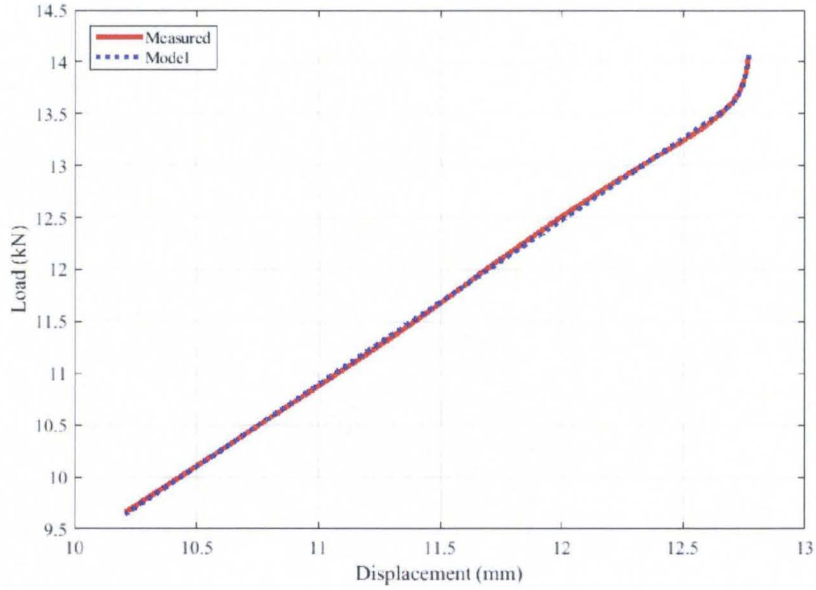

Load vs Displacement Fit (Single Tyre | 20 kN – 10 kN at 25 km/h)

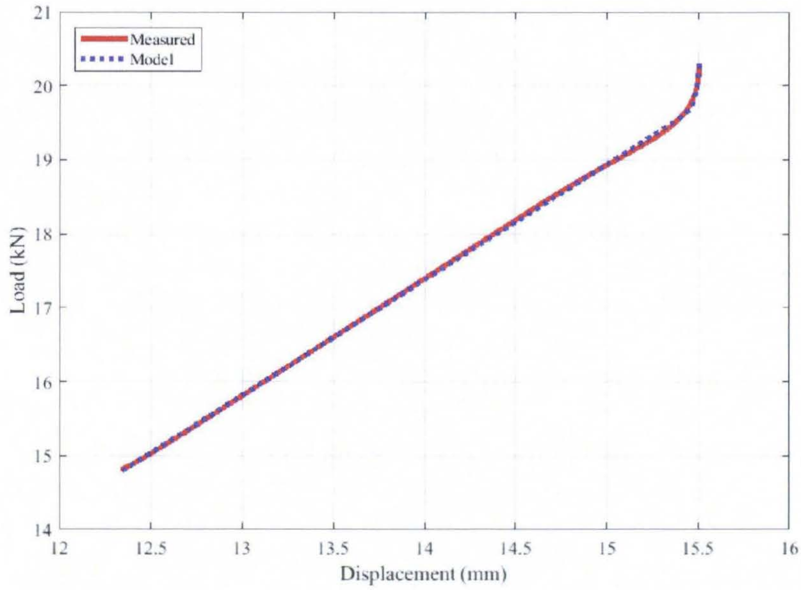

Load vs Displacement Fit (Single Tyre | 30 kN – 20 kN at 25 km/h)

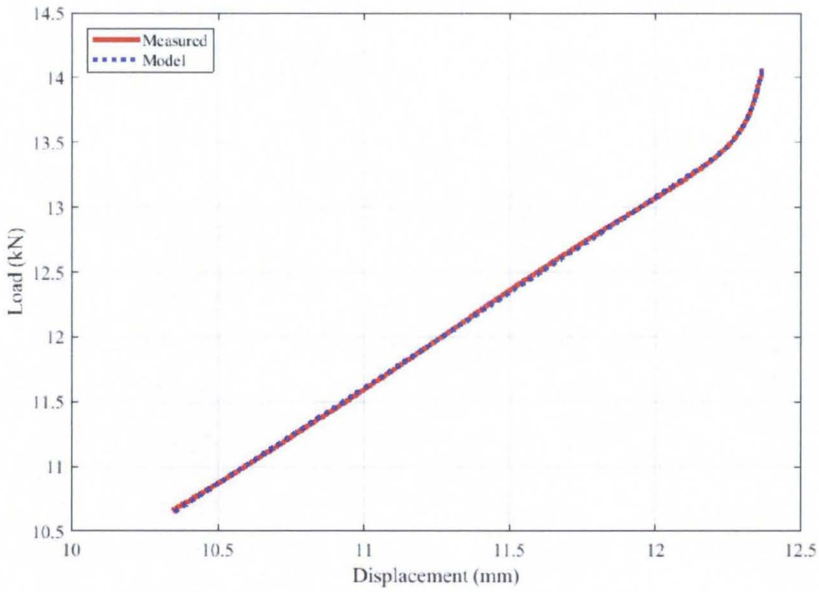

Load vs Displacement Fit (Single Tyre | 20 kN – 10 kN at 35 km/h)

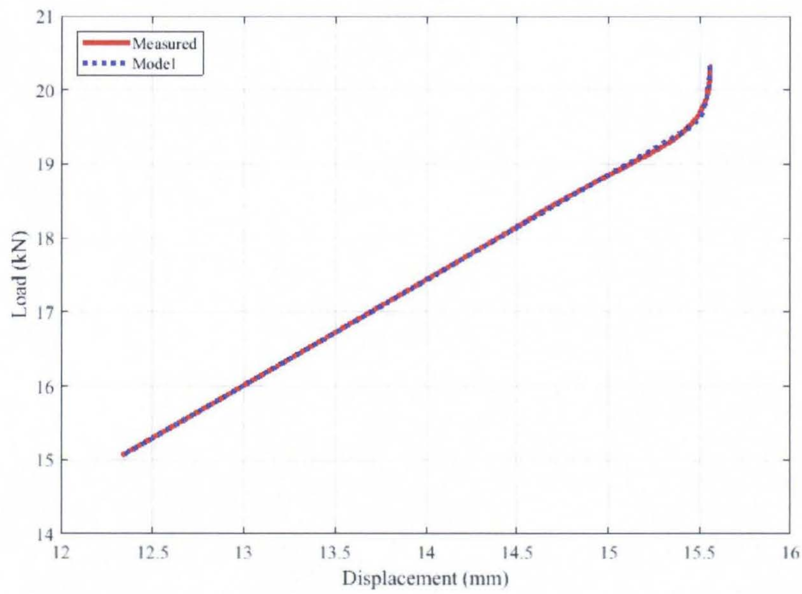

Load vs Displacement Fit (Single Tyre | 30 kN – 20 kN at 35 km/h)

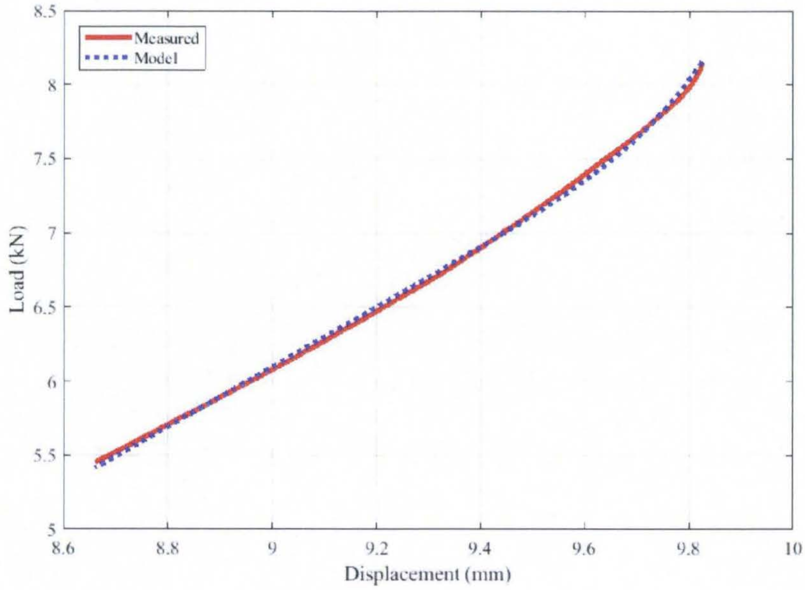

Load vs Displacement Fit (Dual Tyre | 10 kN – 3 kN at 0 km/h)

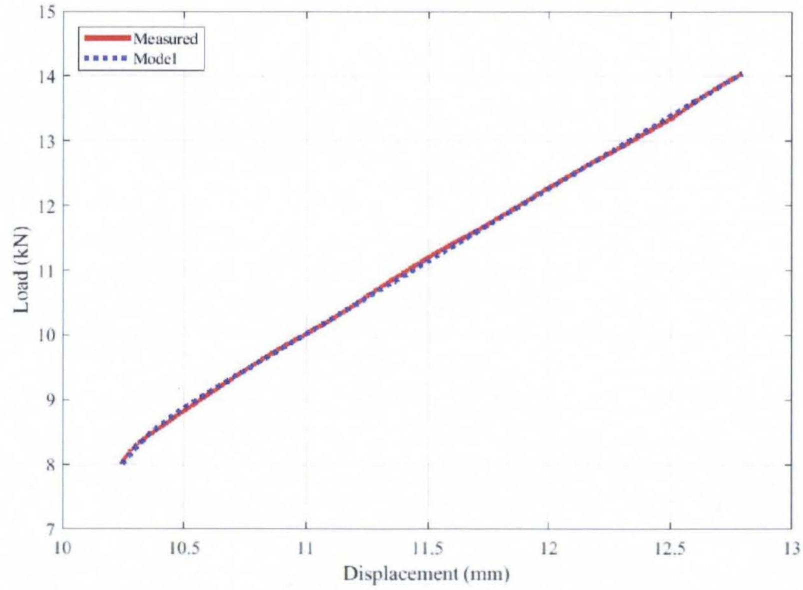

Load vs Displacement Fit (Dual Tyre |10 kN – 20 kN at 0 km/h)

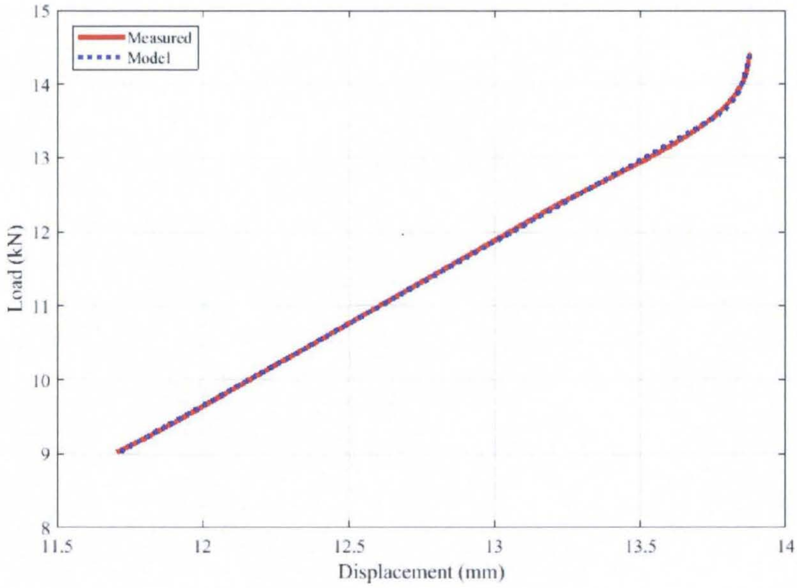

Load vs Displacement Fit (Dual Tyre | 20 kN – 10 kN at 0 km/h)

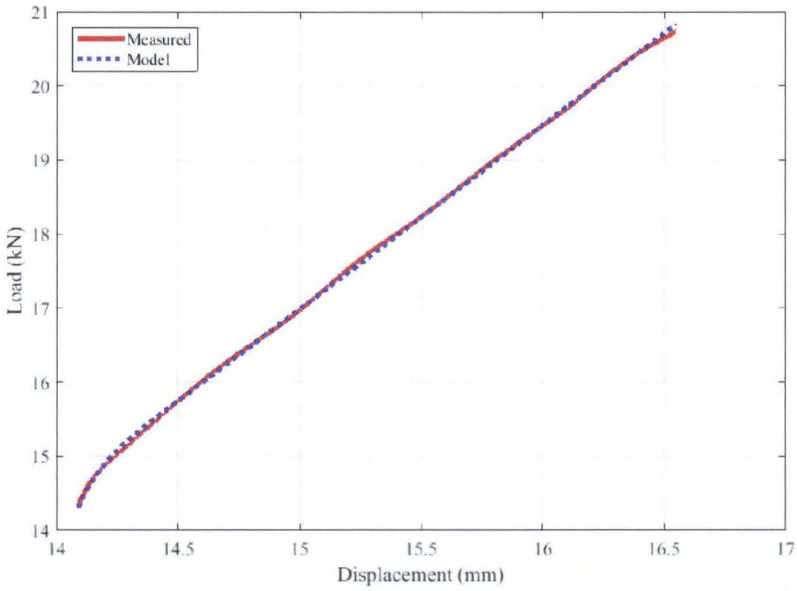

Load vs Displacement Fit (Dual Tyre | 20 kN – 30 kN at 0 km/h)

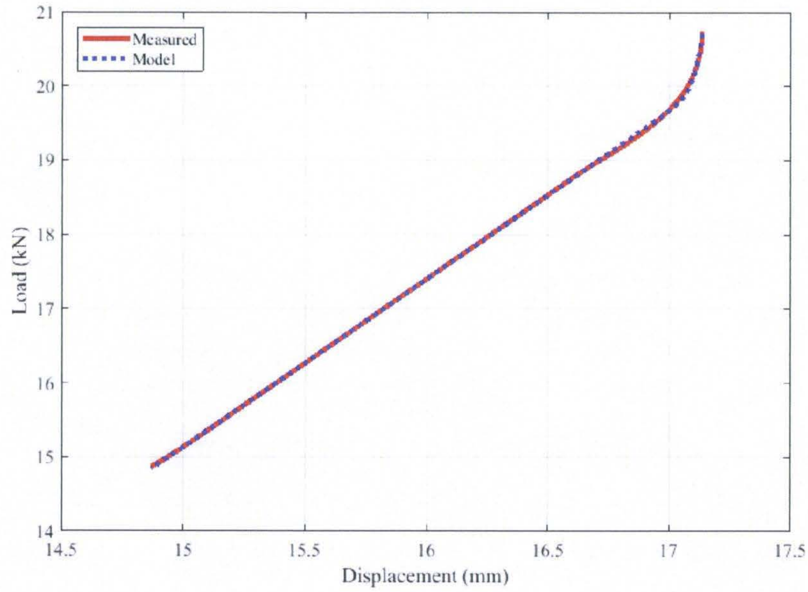

Load vs Displacement Fit (Dual Tyre | 30 kN – 20 kN at 0 km/h)

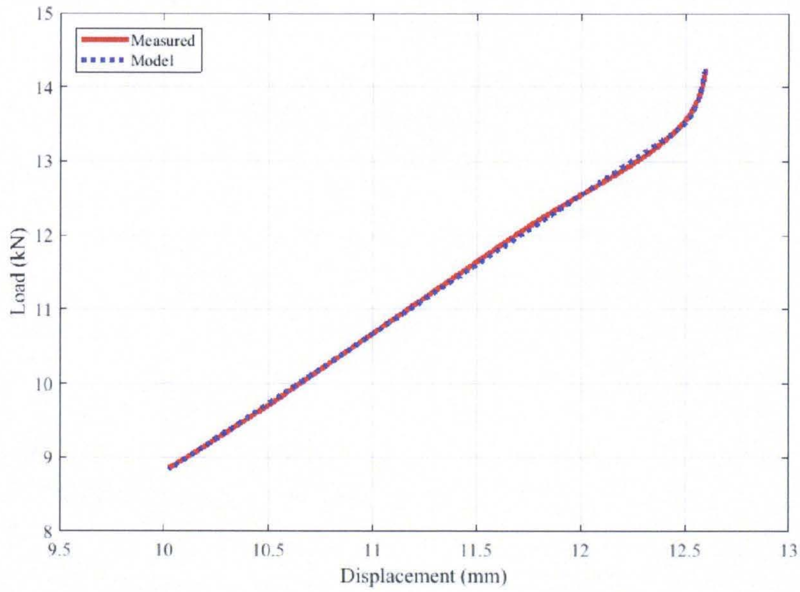

Load vs Displacement Fit (Dual Tyre | 20 kN – 10 kN at 15 km/h)

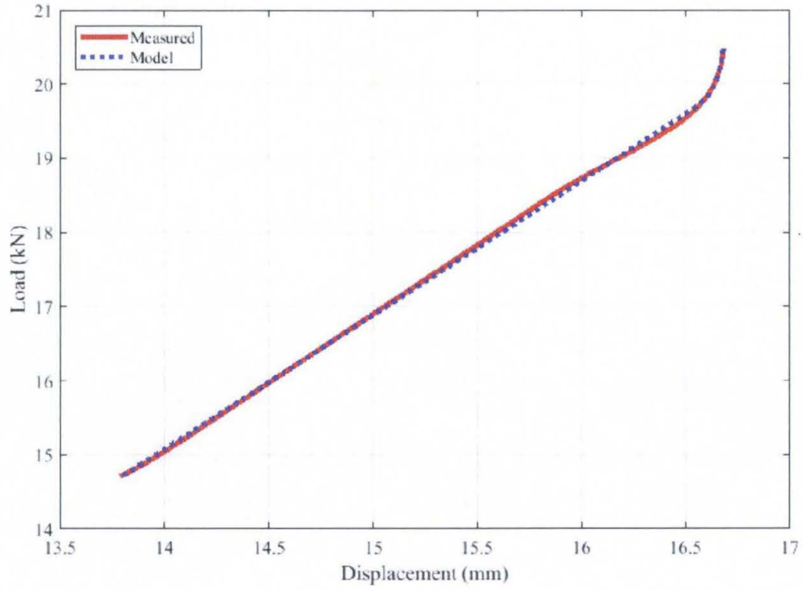

Load vs Displacement Fit (Dual Tyre | 30 kN – 20 kN at 15 km/h)

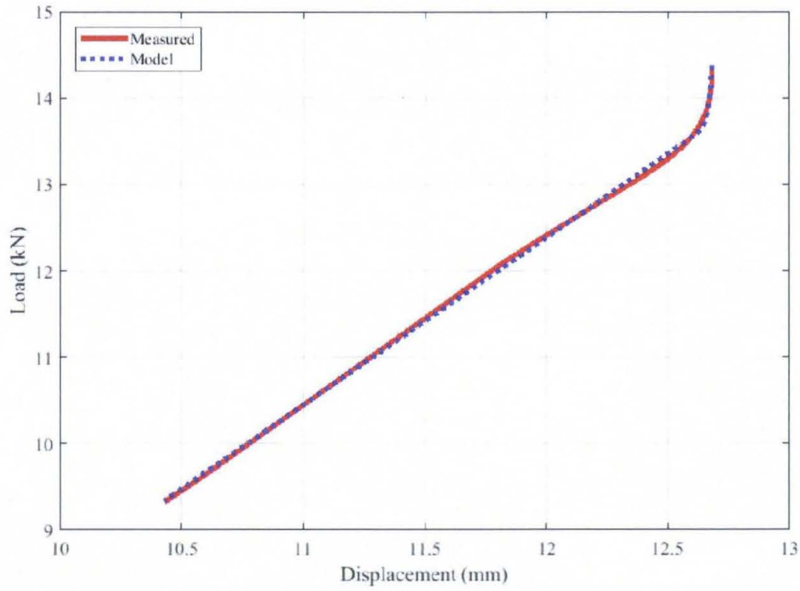

Load vs Displacement Fit (Dual Tyre | 20 kN – 10 kN at 25 km/h)

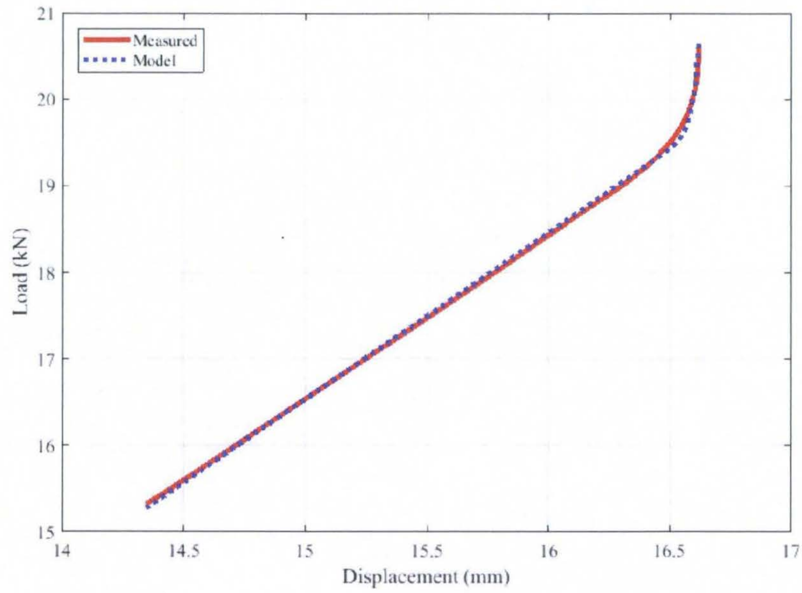

Load vs Displacement Fit (Dual Tyre | 30 kN – 20 kN at 25 km/h)

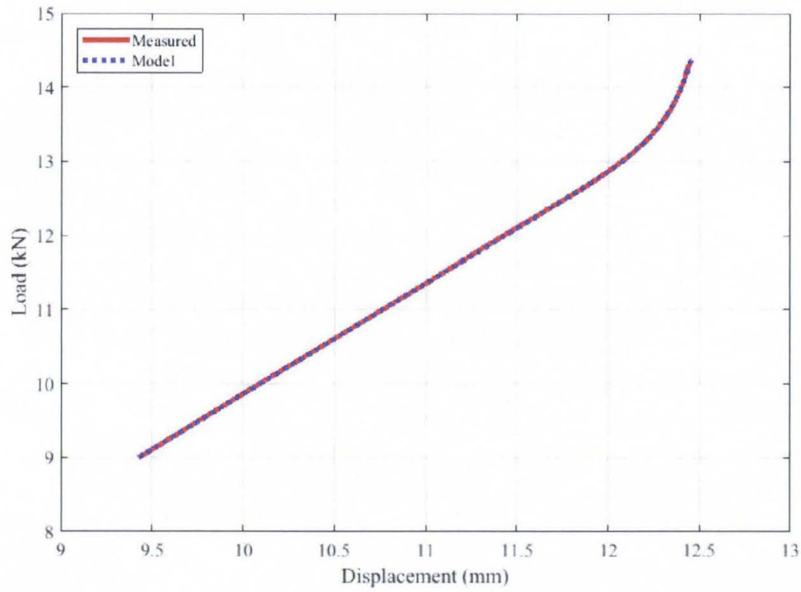

Load vs Displacement Fit (Dual Tyre | 20 kN – 10 kN at 35 km/h)

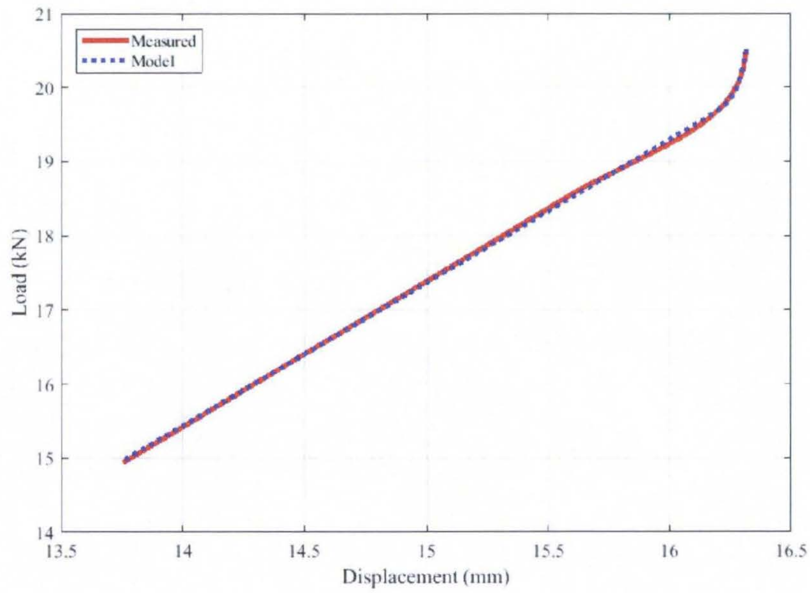

Load vs Displacement Fit (Dual Tyre | 30 kN – 20 kN at 35 km/h)